CHAPTER 5

Chemical assessment of three Octahedral Ni(II) Complexes with heterocyclic Acylpyrazolone ligand: Crystal structure, DFT-NBO analysis, Hirshfeld and Magnetic study

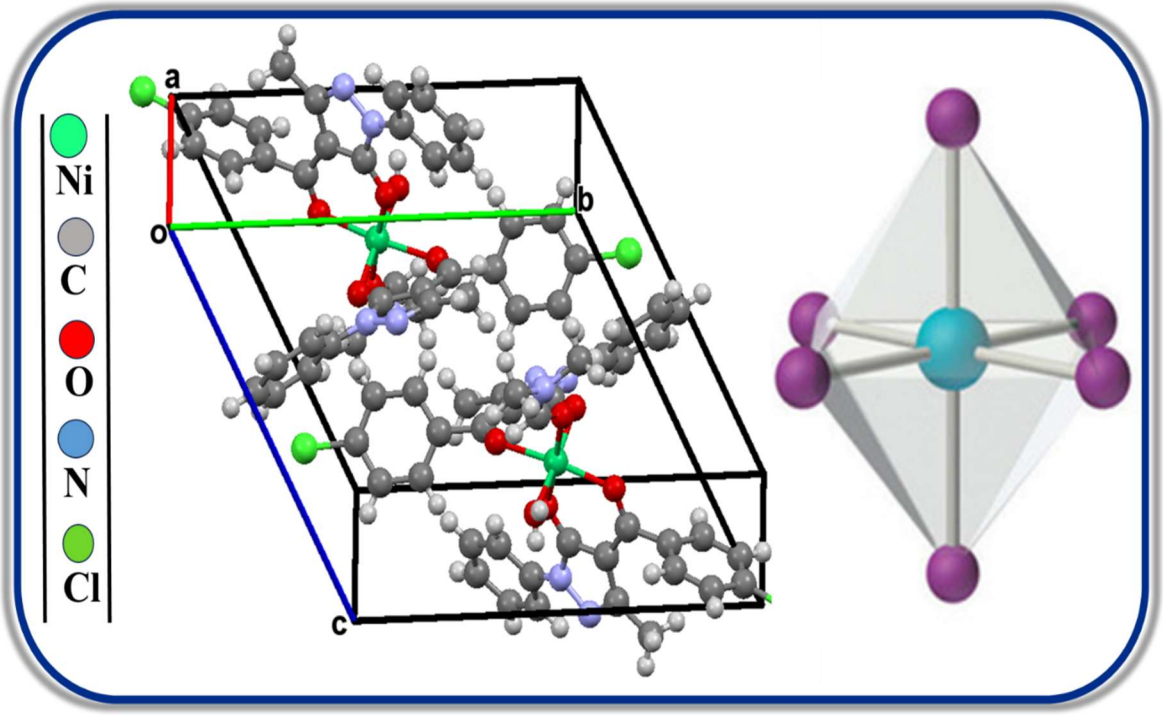

5.1 Introduction

The catalytic and bioinorganic significance of transition metal complexes has sparked considerable interest in their chemistry. Coordination compounds, which form coordinate bonds with donor atoms like sulfur, oxygen and nitrogen, have a rich history [1]. Coordination chemistry involves metal ions accepting electron pairs from adjacent ligands. Due to their potential applications in magnetic ordering, catalysis and biological mimicking, significant research has been dedicated to synthesizing and characterizing polynuclear transition metal complexes and examining their magnetic and electronic properties over the past few decades [2].

In many fields of material chemistry, Nickel is an essential metal. The ceramics production using Nickel-containing alkoxides involves contemporary interactions between Nickel coordination chemistry and material science. This process utilizes the distinctive properties of Nickel alkoxides to create advanced ceramic materials [1]. However, It is well known that pure inorganic Nickel salts or the dehydroacetic acid ligand alone are less active than Nickel complexes containing Ni^{2+} [2]**.** Being more stable than Ni(0), Ni(I), Ni(III) and Ni(IV), Nickel is commonly found in nature as Nickel(II). In recent years, the coordination chemistry of pyrazoles and other nitrogen-containing heterocyclic compounds has garnered significant attention. It has been extensively applied in the fields of transition metal chemistry, bioinorganic chemistry and organometallic chemistry [3]**.**

In the pharmaceutical sector, pyrazole derivatives are employed as medication ingredients or as additives in herbicides and antifungal agents due to their well-known complex properties [4]. The first Ni(II) 4-aminoalkylidene-5-pyrazolone compounds were octahedral dihydrate paramagnets with two unpaired electrons [5]**.** Over the past fifty years, the rich electronic structure of octahedral Ni(II) complexes has been investigated for a variety of purposes, from the application of crystal field theory in inorganic coordination chemistry to contemporary photophysical phenomena like visible to near-infrared upconversion. The critical experimental data required to create and evaluate models and concepts for these domains is provided by the d–d transitions seen in the absorption spectrum [6]**.** Transition metal atoms can be coordinated with ligands that include a range of donor atoms, such as oxygen, nitrogen and sulphur. Transition metal complexes exhibit different coordination modes with varying degrees of distortion depending on the nature of the potential counter ion. They can be bidentate, tridentate, tetradentate, or polydentate, depending on the type and oxidation state of the central metal atom and the ligand

structure. Transition metal complexes also display a variety of coordination modes with different levels of deformation [7].

Cu(II) complexes have already been reported for their synthesis and characterization in our previously published articles (Chapters **3** and **4**) [8][9][10]. Nickel has been selected for complexation and subsequent characterization. Our investigation focuses on the synthesis and structural properties of Ni(II) complexes, including their crystal structures, spectral data, and magnetic characteristics. This study builds upon and extends our previous research in this area.

Furthermore, several relevant quantum parameters were quantified using density functional theory (DFT) to support this work. The structural and spectroscopic properties of the synthesized molecule were predicted through Hirshfeld surface analysis and HOMO/LUMO energy calculations. Magnetic studies demonstrated the paramagnetic behaviour of the compounds.

5.2 Experimental Section

5.2.1 Materials and Methods

The Nickel salts, AR-grade solvents and pyrazolone material were obtained from the same suppliers mentioned in Chapters **2** and **3.**

5.2.2 Synthetic route of complex-9, complex-10 and complex-11

In the synthesis of the Nickel complexes, hot ethanolic solution of the HL^{VIII} ligand (0.6403g, 0.002 mol), HL^{IV} ligand (0.625g, 0.002 mol) and HL^{VI} ligand (0.653g, 0.002 mol) were taken in three different round-bottom flasks each fitted with a water condenser in a closed system. The ligands HL^{VIII}, HL^{IV} and HL^{VI} were synthesized as detailed in Chapter **2**, following methods previously reported by our lab [11][12][13]. These ligands served as starting materials to synthesize three new Ni(II) complexes. Nickel metal salt (0.248g of $Ni(OOCCH_3)_2.4H_2O$, 0.001mol) dissolved in CH_3CH_2OH (10 mL) was subsequently added to the ethanolic solution of HL^{VIII} ligand. Other Nickel metal salt (0.262g of $NiSO_4.6H_2O$, 0.001mol) dissolved in CH_3CH_2OH (10 mL) was then added to the ethanolic solution of HL^{IV} ligand and HL^{VI} ligand in two different RB flasks. The resulting mixture was refluxed for eight to ten hours at 80-90°C temperature in three separate RB flasks. Clear solutions of all three complexes were obtained and kept at room temperature for one to two weeks as the complexes formed through slow evaporation. Pale green precipitates of the synthesized Nickel complexes were produced. The obtained

products were filtered using Whatman filter paper 1, washed with warm ethanol and dried. A small portion of each complex was taken for analysis, while the remaining amount was kept for recrystallization. Complex-**9**, complex-**10** and complex-**11** were dissolved in hot EtOH, DMF and DMSO solvents, respectively for recrystallization. After few days, X-ray-quality single green crystal of $[Ni(HL^{VIII})_2(EtOH)_2]$ complex-**9,** $[Ni(HL^{IV})_2(DMF)(H_2O)]$ complex-**10** and $[Ni(HL^{VI})_2(DMSO)_2]$ complex-**11** were obtained.

HL^{VIII} ligand: (0.6403g, 0.002 mol): M.P: 134°C, Molecular formula: $C_{20}H_{20}N_2O_2$, M.W: 320.15.

HL^{IV} ligand: (0.625g, 0.002 mol): M.P:105°C, Molecular formula: $C_{17}H_{13}ClN_2O_2$, M.W: 312.75.

HL^{VI} ligand: (0.653g, 0.002 mol), M.P:108°C, Molecular formula: $C_{18}H_{15}ClN_2O_2$, M.W: 326.78.

Complex-9: Pale bluish green crystal, yield: 81%, M.P:> 200°C, Molecular formula: $C_{44}H_{50}N_4NiO_6$, **M.W**: 789.58, **Elemental analysis**: C (Exp. 65.39%, Calc. 66.9%); H (Exp. 6.3%, Calc. 6.3%); N (Exp. 8.23%, Calc. 7.54%); Ni = 8.4% (Metal estimation-gravimetrically and volumetrically), **FTIR(KBr, cm^{-1}):** ν(C=O) of pyrazolone: (1596), ν(C=O) of benzoyl chloride: (1558), cyclic ν(C=N): (1486).

Complex-10: Pale green crystal, yield: 81%, M.P:> 200°C, Molecular formula: $C_{38}H_{36}Cl_2N_5NiO_6$, **M.W**: 788.32, **Elemental analysis**: C (Exp. 57.39%, Calc. 58.10%); H (Exp. 4.20%, Calc. 4.60%); N (Exp. 8.23%, Calc. 8.88%); Ni = 8.6% (Metal estimation-gravimetrically and volumetrically), **FTIR(KBr, cm^{-1}):** ν(C=O) of pyrazolone: (1613), ν(C=O) of benzoyl chloride: (1590), cyclic ν(C=N): (1457).

Complex-11: Pale yellow-green crystal, yield: 83%, M.P:> 200°C, Molecular formula: $C_{42}H_{46}Cl_2N_4NiO_6S_2$, **M.W**: 896.57, **Elemental analysis**: C (Exp. 55.92%, Calc.: 56.26%); H (Exp. 5.10%, Calc. 5.15%); N (Exp. 6.10%, Calc. 6.25%); Ni = 8.4% (Metal estimation gravimetrically and volumetrically), **FTIR(KBr, cm^{-1}):** ν(C=O) of pyrazolone: (1602), ν(C=O) of benzoyl chloride: (1540), cyclic ν(C=N): (1159).

The mass spectrum of complex-9 is depicted in **Fig.5.1** and a synthetic pathway of complexes **9, 10** and **11** is demonstrated in **Fig.5.2.** The physical appearance of three synthesized Nickel complexes is pictured in **Fig.5.3**.

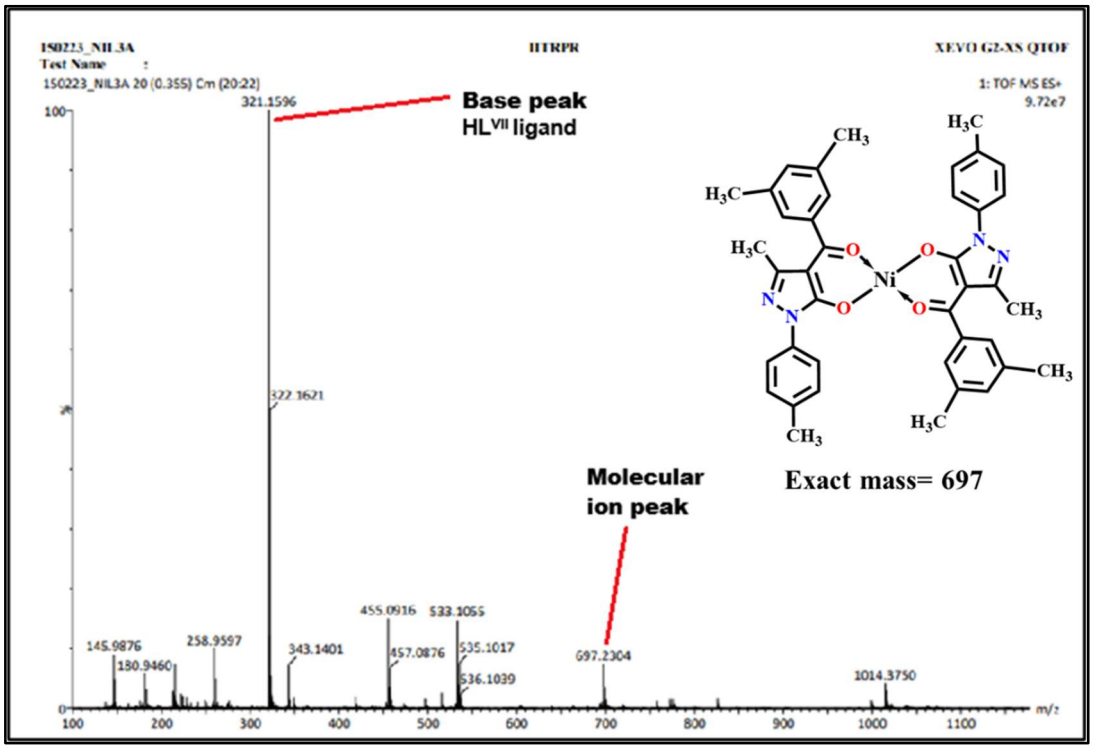

Fig.5.1. Mass spectrum of complex-9

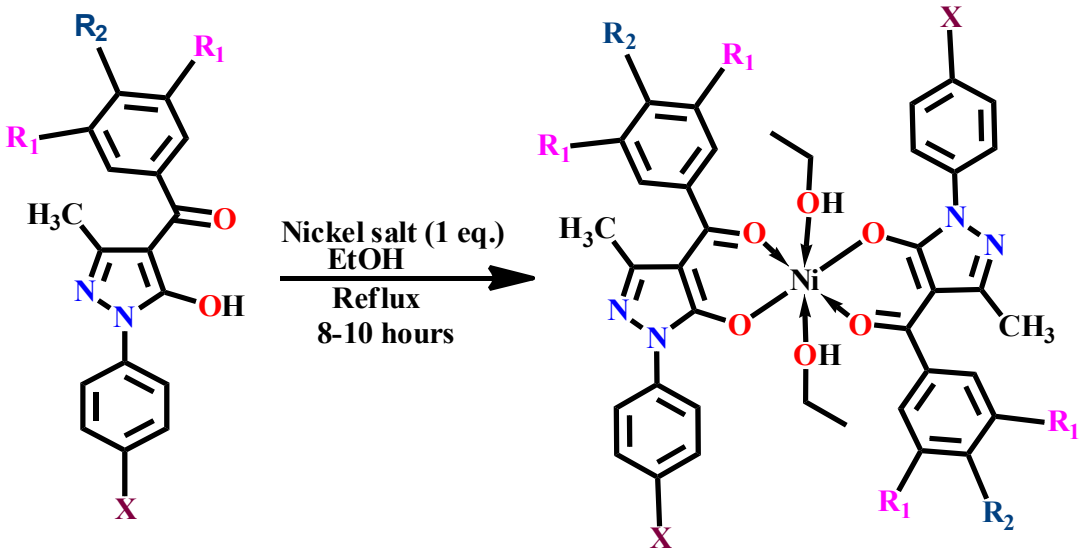

Complex-9: R_1= CH_3, R_2= H, X= CH_3
Complex-10: R_1= H, R_2= Cl, X = H
Complex-11: R_1= H, R_2=Cl, X= CH_3

Fig.5.2. Synthetic pathway of complex-9, complex-10 and complex-11

Complex-9 Complex-10 Complex-11

Fig.5.3. Physical appearance of complex-9, complex-10 and complex-11

5.2.3 X-ray crystallographic structure determination

All the Ni(II) complexes were synthesized in hot ethanol, and X-ray quality single crystals of complex-**9**, complex-**10**, and complex-**11** were obtained using EtOH, DMF, and DMSO solvents, respectively. Data for complex-**9** were collected at 298(2) K on a Bruker D8 Venture diffractometer using graphite monochromated Cu—Kα (λ=1.54178 Å) radiation. Data for complex-**10** and complex-**11** were collected at 100(2) K on a Bruker APEX-II CCD diffractometer and Cu—Kα (λ = 1.54184 Å) radiation. In complex-**9**, coordinated ethanol molecules exhibit disorder over two positions, with the aliphatic chain components having refined occupancies of 0.510(8):0.490(8) and 0.562(11):0.438(11). The data were integrated with SAINT and afterwards, multi-scan absorption corrections were applied using SADABS. Structure solutions by direct methods, full-matrix least-squares refinement based on F^2 [14][15][16]. All but H-atoms were refined anisotropically, hydrogen atoms were located from different Fourier maps, refined at idealized positions riding on the carbon atoms with isotropic displacement parameters Uiso(H) = 1.2Ueq(C) or 1.5Ueq(CH_3) and C-H 0.95- 0.98 Å. For 1 H(water), positions were refined freely. All CH_3 hydrogen atoms were allowed to rotate but not to tip. Mercury software was employed for the ORTEP views of all three complexes [17].

5.2.4 Physical measurements and characterization

Spectroscopic and analytical methods were used to investigate all three synthesized Ni(II) complexes. The complexes were characterized by FTIR (4000–400 cm^{-1}, KBr discs), UV-Vis, TG-DTA and X-ray single crystal analysis. A magnetic study was conducted at IISER Bhopal using a SQUID-VSM magnetometer to analyze the magnetic properties of the compound. Molar conductivity was measured using an EQ-664A model in a 10^{-3} M DMF solution at room temperature. Elemental analysis of all three complexes was carried

out using the Elementar Excellence in Elements model Unicube superuser V1.3.2 (065bdfa). The mass spectrum was recorded at IIT Ropar using an XEVO G2-XS QTOF. The electronic spectra of the complexes were recorded on a V-730 model spectrophotometer. The Nickel content in each complex was determined through gravimetric and volumetric analysis following decomposition with HNO_3.

5.2.5 Computational measurements (DFT)

Complexes were subjected to thorough geometry optimizations at the B3LYP/LANL2DZ level basis set via the density functional theory (DFT). This study was conducted to ensure that the resultant structures were in the least energy state [20][21]. The computational analysis was entirely done on Gauss View 6.0 software [18]. HOMO-LUMO energies analysis and NBO calculations were carried out theoretically. The NBO analysis was performed to explain how occupied and empty Lewis orbitals of the NBO type interact.

5.2.6 Magnetic study

The magnetic properties of the compound were looked over at IISER Bhopal using a SQUID-VSM magnetometer at ZFC (zero-field cooling) and FC (field colling) at 500 Oe(0.05T).

5.3 Results and Discussion

All the nickel complexes have been synthesized using a general method. They are stable at room temperature. FT-IR, UV-Vis, TGA, UV-Vis, X-ray crystallography, Powder XRD and Magnetic study techniques were used to characterize the complexes. Three Ni(II) complexes have been discussed below using different characterization and analytical methods.

5.3.1 FTIR spectral analysis

The IR frequencies of benzoyl chloride ν(C=O) and pyrazolone ν(C=O) are observed at 1558 cm^{-1} and 1596 cm^{-1} for complex-**9**. Meanwhile, 1590 cm^{-1} and 1540 cm^{-1} IR frequencies are attributed to ν(C=O) of benzoyl chloride of complex-**10** and complex-**11**, respectively. For ν(C=O) pyrazolone, the observed IR frequencies are 1613 cm^{-1} and 1602 cm^{-1} for complex-**10** and complex-**11**, respectively. When the metal complexes form, a noticeable drop in IR frequencies is observed compared to the free ligands. This change is attributed to the strengthening of the M-O bond, which occurs alongside the weakening of the C-O bonds due to charge transfer from the molecule to the metal ions during

complexation. In all three synthesized complexes, the ν(C=O) IR frequencies of the pyrazolone group are higher than those of benzoyl chloride. This is because the electrons from the C=O group in pyrazolone actively participate in bonding with the metal centre, which strengthens the M-O bond and weakens the C=O bond in pyrazolone. As a result, the C=O bond length increases [19]. FTIR spectra of complexes **9**, **10** and **11** are depicted in **Figs.5.4-5.6,** respectively. FTIR frequencies of all three complexes are listed in **Tables 5.1-5.3.**

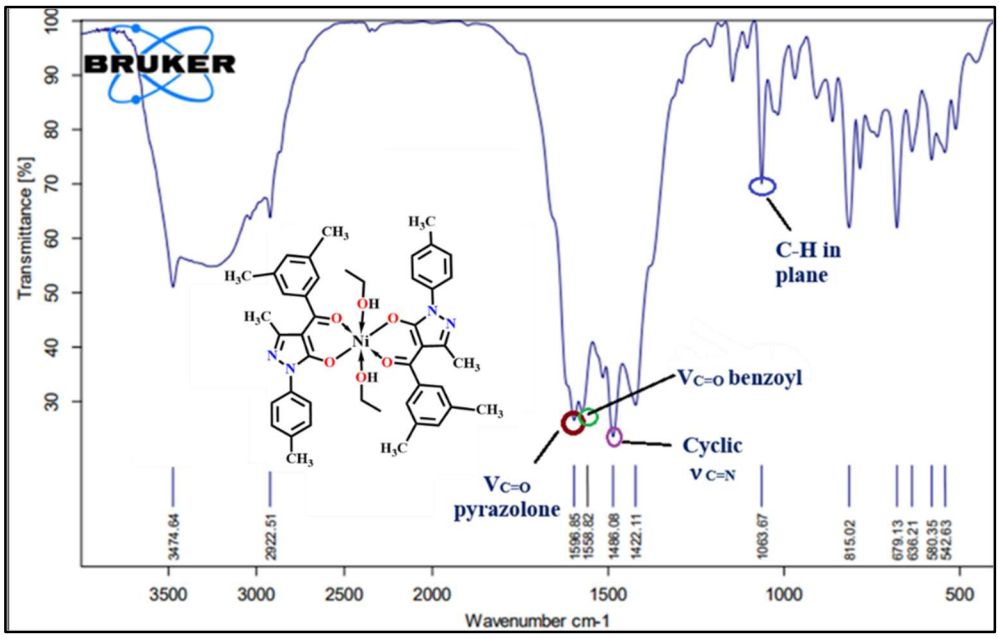

5.4. FTIR spectrum of complex-9

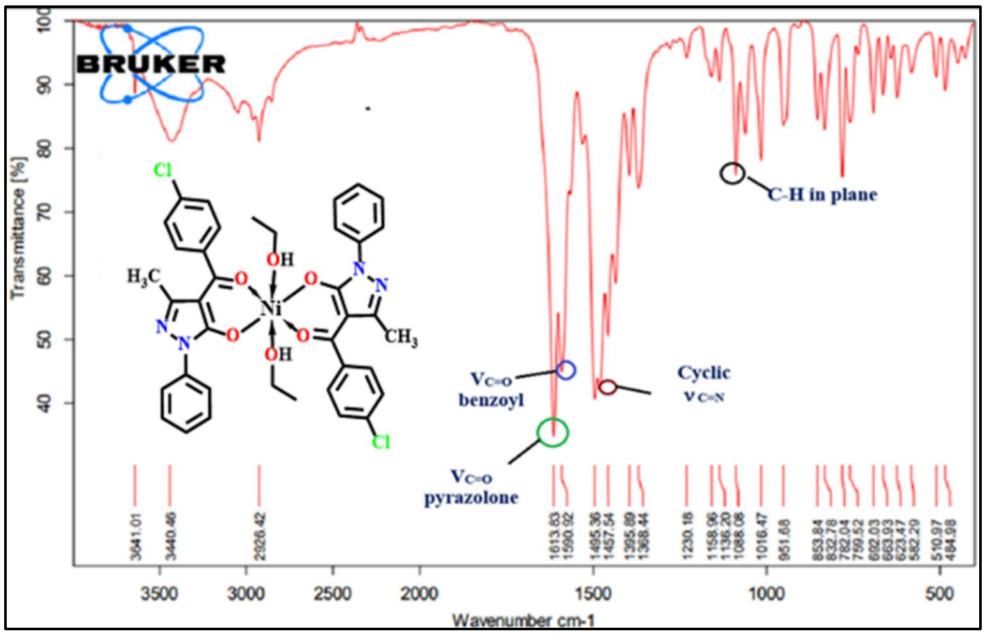

Fig.5.5. FTIR spectrum of complex-10

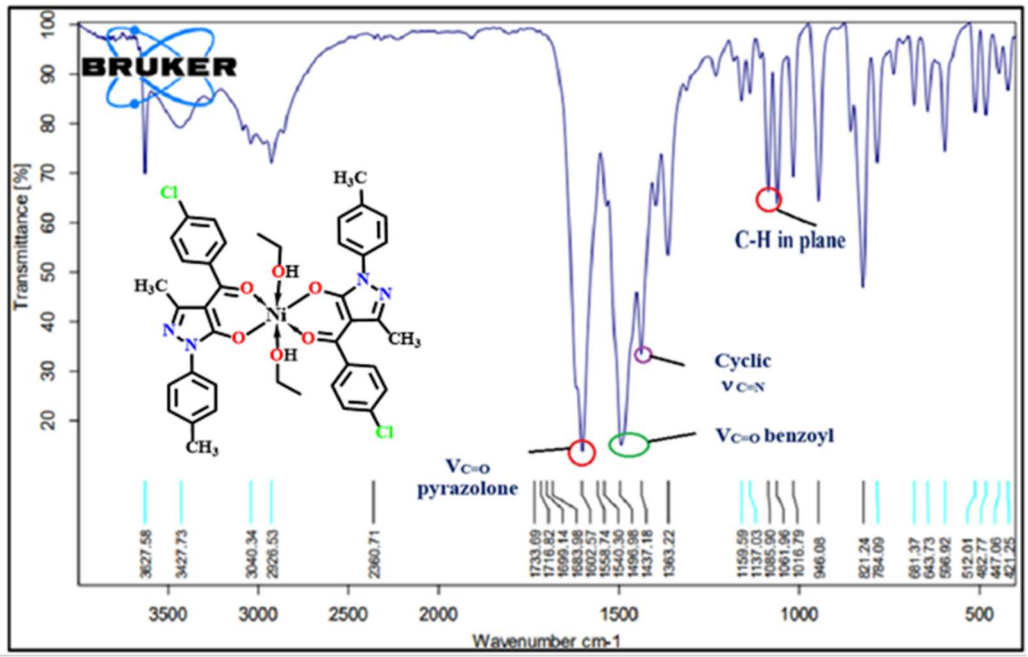

Fig.5.6. FTIR spectrum of complex-11

Table 5.1. FTIR spectral data of ligand and complex-9

Code	HL^{VIII} ligand	Complex-9
ν(C=O) of benzoyl chloride	1606	1558
Cyclic ν(C=N)	1400	1486
ν(C=O) of Pyrazolone	1620	1596
C–H in-plane deformation	1175	1063
ν_{M-O}	-	580

Table 5.2. FTIR spectral data of ligand and complex-10

Code	HL^{IV} ligand	Complex-10
ν(C=O) of benzoyl chloride	1588	1590
Cyclic ν(C=N)	1459	1457
ν(C=O) of Pyrazolone	1619	1613
C–H in-plane deformation	1213	1158
ν_{M-O}	-	582

Table 5.3. FTIR spectral data of ligand and complex-11

Code	HL^{VI} ligand	Complex-11
ν(C=O) of benzoyl chloride	1551	1540
Cyclic ν(C=N)	1423	1437
ν(C=O) of Pyrazolone	1610	1602
C–H in-plane deformation	1213	1159
ν_{M-O}	-	596

5.3.2 Molar conductivity

In a 10^{-3} M DMF solution, the molar conductivity of all three complexes was measured. Molar conductivity was determined to be 3.10 $ohm^{-1}cm^2mol^{-1}$ and 2.18 $ohm^{-1}cm^2mol^{-1}$, 2.20 $ohm^{-1}cm^2mol^{-1}$ for the complex-**9**, complex-**10** and complex-**11,** respectively. Such lower molar conductivity values imply no counter ion and the complexes have non-electrolytic behaviour [20].

5.3.3 Thermogravimetric analysis

Thermogravimetric analysis, or TGA, describes how the mass of a substance changes as a function of temperature. It is possible to assess a three-step decomposition of the complexes **9, 10** and **11**. All the complexes were synthesized in ethanol solvent. Degradation of a solvent molecule occurs till 200°C. EtOH solvent molecule bound to metal ion is degraded at more than 100°C and EtOH molecule outside the coordination sphere is degraded at less than 100°C in all three complexes. 42.44% EtOH degradation can be observed in the complex-**9**, 14.5% and 12.4% in the complex-**10** and 9.9% in the complex-**11**. Thermal breakdown at temperatures between 100 and 550°C serves as evidence of the remarkable thermal stability of Ni(II) complexes. Two HLV^{II} ligand molecules underwent pyrolysis, resulting in the degradation of the ligand up to 290°C and a loss of 43.85% in complex-**9**. The DTG curve showed a considerable reduction of 0.209 mg/min at 383.8°C. Two HL^{IV} ligands in complex-**10** are pyrolyzed in two steps up to 310°C. The HL^{VI} ligand degrades in two stages in the complex-**11,** with the first degrading at 150°C and the second occurring up to 320°C. For all three complexes, the resultant NiO residue is stable up to 550°C. TG-DTA plots of complex-**9**, complex-**10** and complex-**11** are shown in **Figs.5.7, 5.8** and **5.9,** respectively.

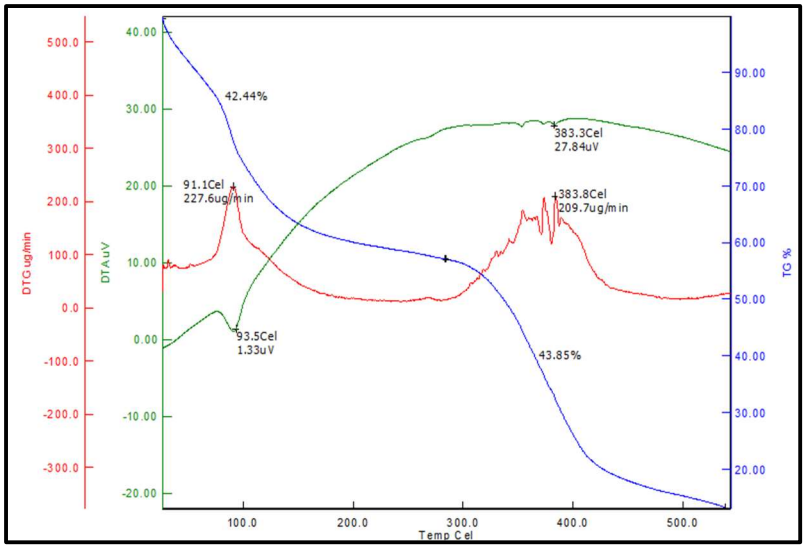

Fig.5.7. TG-DTA plot of complex-9

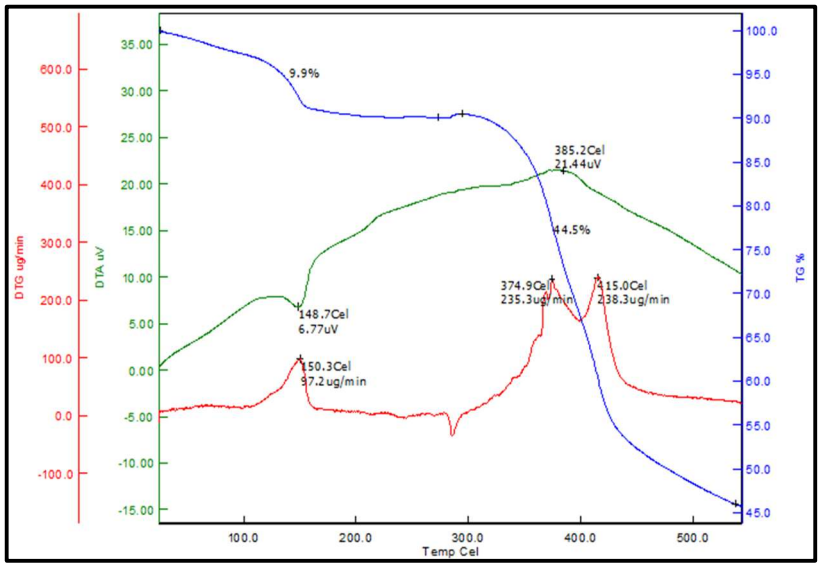

Fig.5.8. TG-DTA plot of complex-10

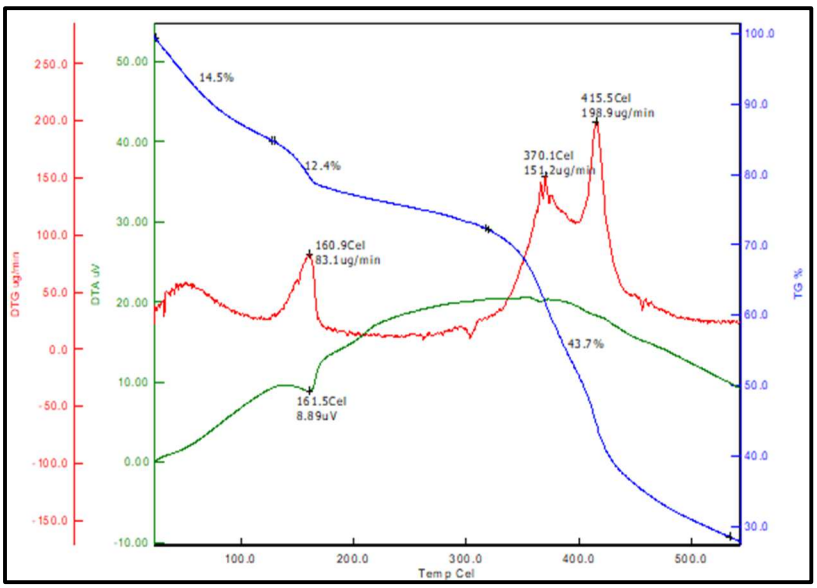

Fig.5.9. TG-DTA plot of complex-11

5.3.4 Electronic spectral analysis

Electronic transition (d-d transition) of complex-**9** and complex-**11** were obtained in a 100% DMSO (1×10^{-3} M) solution up to 950 nm [21]. Meanwhile, d-d bands of complex-**10** were obtained in 10^{-2} M concentration. Charge transfer (LMCT) spectra were recorded in a diluted solution of DMSO. The absorption in the ultraviolet region at 300 nm is assigned to π-π* transitions, while 415 nm is assigned to n-π* transitions in the synthesized complex-**9.** A similar transition can also be seen for complex-**10** at 280 nm attributed to π-π* transitions and at 355 nm attributed to n-π* transitions. While a band at 282 nm is assigned to π-π* transitions and a band at 355 nm is attributed to n-π* transitions in complex-**11**. The electronic transition of all three Ni(II) complexes exhibits three distinct absorption bands in the visible region. Such as, $3A_{2g}\rightarrow3T_{1g}(P)$, $3A_{2g}\rightarrow3T_{1g}(F)$, $3A_{2g}\rightarrow3T_{2g}$ [22][23]. Uv-Vis absorption bands of complex-**9**, complx-**10** and complex-**11** are depicted in **Figs.5.10-5.12.** respectively. Distinct absorption bands and molar absorbance values are defined in **Table 5.4.** The ligand field parameters of complexes are summarized in **Table 5.5.** As shown in the table below, the value of a nephelauxetic parameter (β) is almost the same for all the complexes; hence, all the synthesized Ni(II) complexes have equal covalent character. However, the value of the Racah parameter (B) is somewhat different. According to Racah parameter (B) 827>825>822 for complex-**11**, complex-**9** and complex-**10,** respectively, a complex-**10** is more covalent and less ionic than the other two complexes.

Covalency Order

complex-10> complex-9> complex-11

Ligand field parameters such as Racah parameter (B), Ligand field splitting parameter (Δ_o), and nephelauxetic parameter (β) are calculated by this formula [24][25]. Spin orbit coupling is calculated using the given formula **(1).**

$$\lambda = 2.7\ B^2/10Dq \qquad (1)$$

Table 5.4. Band Assignments of all three Ni(II) complexes

Compounds	Wavelength (λ) & Molar absorbance (ε)		
	$^3A_{2g} \rightarrow {}^3T_{1g}(P)$	$^3A_{2g} \rightarrow {}^3T_{1g}(F)$	$^3A_{2g} \rightarrow {}^3T_{2g}$
Complex-9	516 nm ($1.7\ M^{-1}cm^{-1}$)	652 nm ($4.0\ M^{-1}cm^{-1}$)	773 nm ($0.3\ M^{-1}cm^{-1}$)
Complex-10	502 nm ($2.0\ M^{-1}cm^{-1}$)	669 nm ($3.8\ M^{-1}cm^{-1}$)	752 nm ($1.7\ M^{-1}cm^{-1}$)
Complex-11	512 nm ($2.0\ M^{-1}cm^{-1}$)	652 nm ($3.0\ M^{-1}cm^{-1}$)	770 nm ($0.5\ M^{-1}cm^{-1}$)

Table 5.5. Ligand-Field Parameters of all three Ni(II) complexes

Compounds	Ligand field parameters			
	B cm^{-1}	β cm^{-1}	Δ_o cm^{-1}	λ
Complex-9	825	0.763	8250	142
Complex-10	822	0.761	8220	137
Complex-11	827	0.765	8270	142

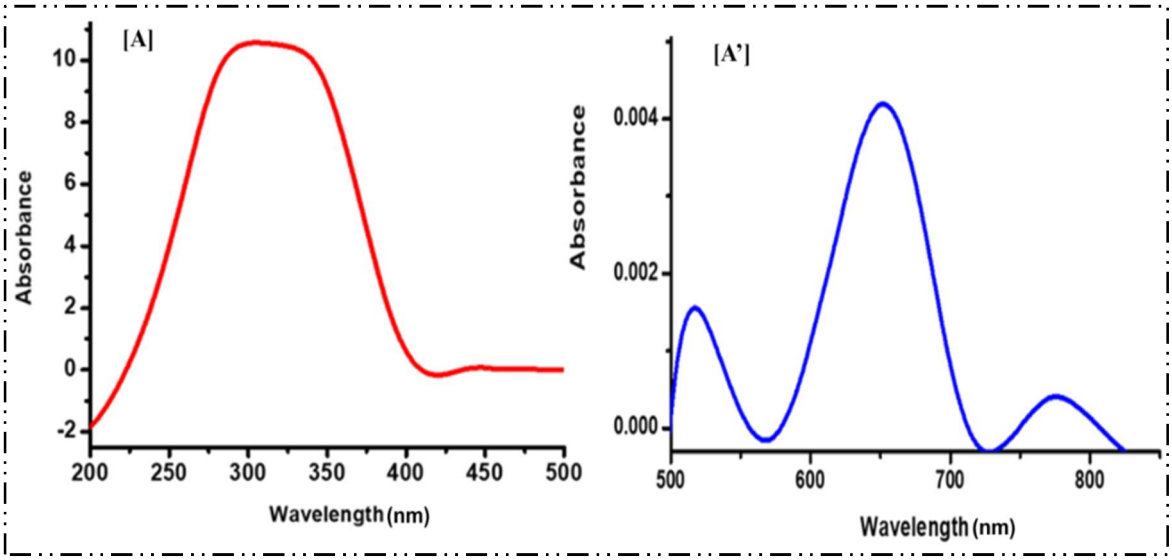

Fig.5.10. (A)= LMCT spectrum of complex-9 in a diluted solution of DMSO

(A')= d-d transition of complex-9 in a $1x10^{-3}$ M solution of DMSO

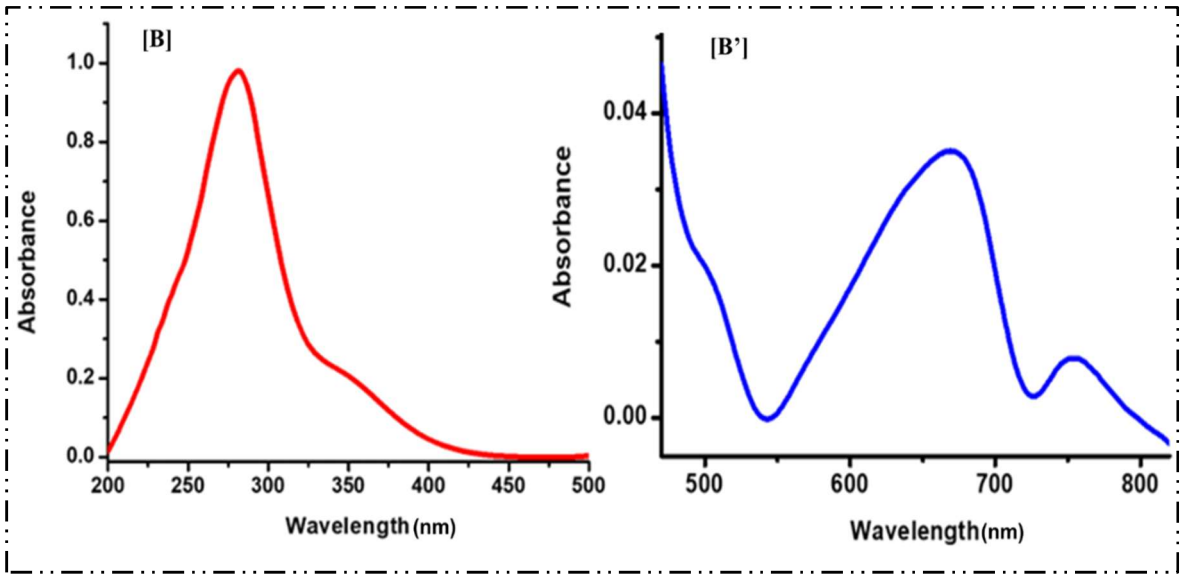

Fig.5.11. (B)= LMCT spectrum of complex-10 in a diluted solution of DMSO

(B')= d-d transition of complex-10 in a $1x10^{-2}$ M solution of DMSO

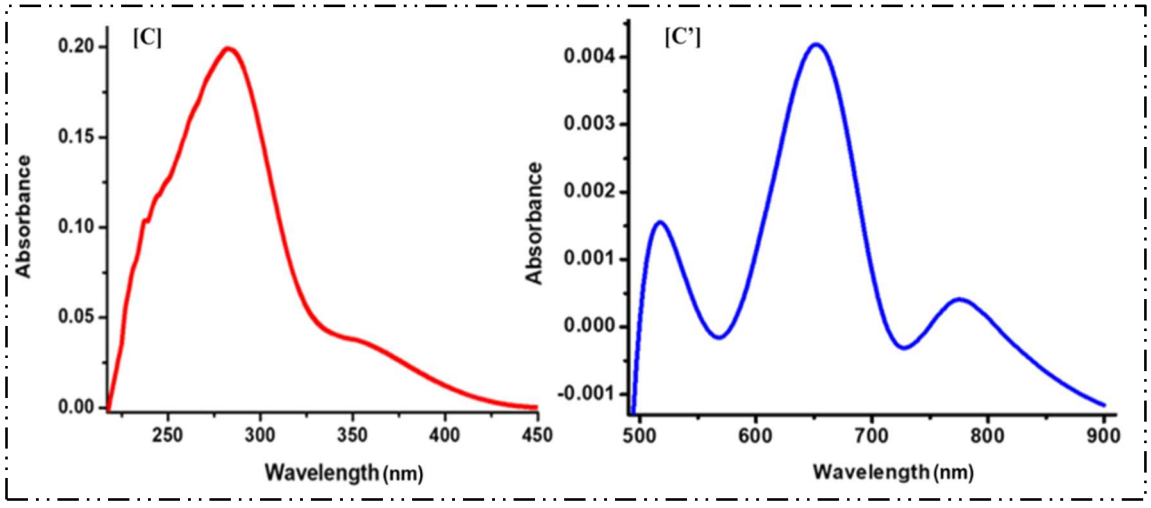

Fig.5.12. (C)= LMCT spectrum of complex-11 in a diluted solution of DMSO

(C')= d-d transition of complex-11 in $1x10^{-3}$ M solution of DMSO

5.3.5 Magnetic study

A superconducting quantum interference (SQUID) device is used to study a material's magnetic characteristics at different magnetic fields and temperatures. Temperature-dependent magnetisation data at 500 Oe (0.05T) was obtained using SQUID. The statistics collected at the ZFC (zero-field cooling) and FC (field colling) do not show any differences. Curie's Law states that the magnetization of a paramagnetic substance is inversely proportional to its temperature, meaning that as the material's temperature rises, magnetization decreases [26].

$$M = C(B/T)$$

C = Curie constant

T = temperature in Kelvin and

B = applied magnetic field

According to Curie–Weiss paramagnetism, magnetic materials may experience a symmetry-breaking transition to a magnetically ordered state at a temperature that corresponds to the strength of the magnetic correlations. Magnetic susceptibility is inversely proportional to temperature; hence, by increasing temperature, the susceptibility decreases. When compared to other temperature-independent contributions to susceptibility, Curie-Weiss susceptibility resulting from paramagnetic local moments usually exceeds one order of magnitude and ranges as 1/T [27]. Here, positive magnetic susceptibilities compatible with its paramagnetic state have been found [2]. Ni(II) complexes **9, 10** and **11** have enough similarities in their characteristics and electronic absorption and hence, only $[Ni(DMBPTMP)_2(EtOH)_2]$ complex has been taken for Magnetic study. The paramagnetic curve of the octahedral Ni(II) complex is depicted in **Figs.5.13** and **5.14.** respectively.

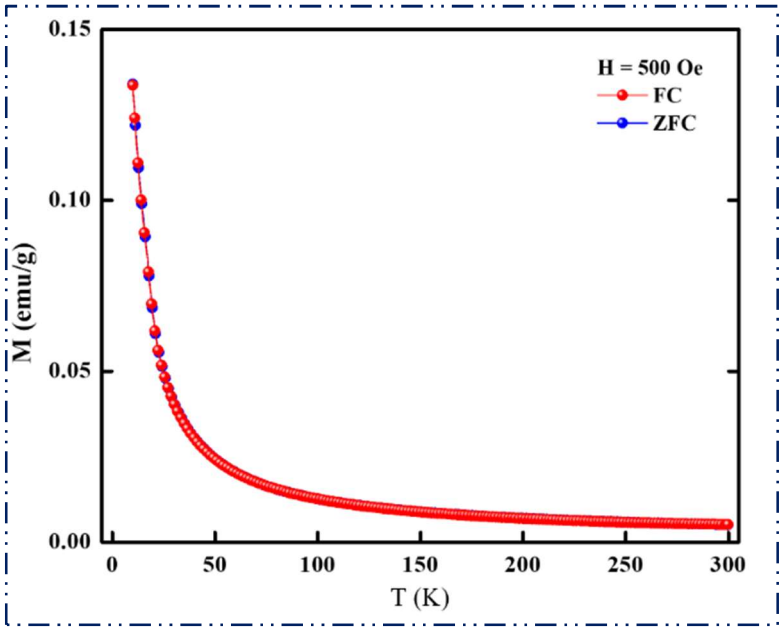

Fig.5.13. Temperature-dependent magnetisation graph at 500Oe measured upon ZFC and FC

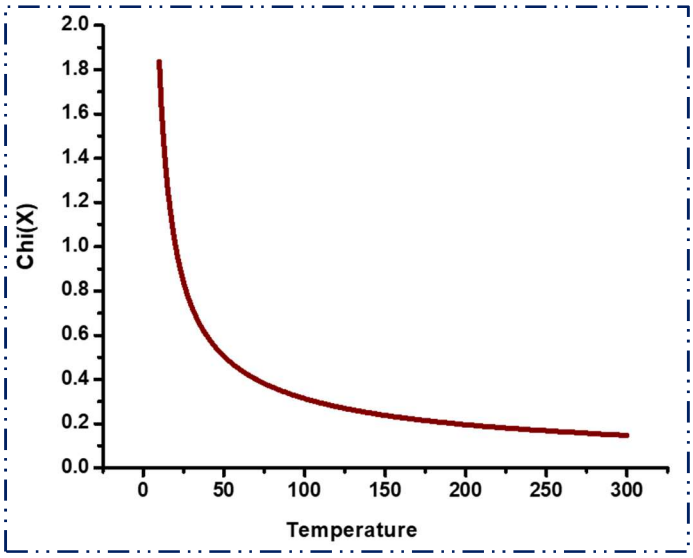

Fig.5.14. Appearance of Curie–Weiss behaviour in direct and inverse susceptibility

5.3.6 Structural properties

The structural analysis evidenced that the Ni centre is 'octahedrally coordinated' from each of the six oxygen atoms in three complexes. Complex-**9** and complex-**10** crystallize in a '**Triclinic crystal system'** with space group *P*-1, while complex-**11** crystallizes in a '**Monoclinic crystal system'** with space group $P2_1/n$. In the latter, the metal is located on a crystallographic inversion centre (Wyckoff position 2a) so that the asymmetric unit is only half the complex. **Table 5.12.** reports the crystal data and details of refinement for the present complexes. The molecular structure and a perspective view of the crystal packing plot of complexes are shown in **Figs.5.15-5.17.** respectively. The Ni-O bond lengths are closely comparable in the three complexes, varying in the range 2.0054(10)-2.0933(12), 2.0167(12)-2.0761(12) and 2.0340(15)-2.0884(15) Å, respectively. In complex-**9**, a HLV^{III} ligand coordinates the metal with chelating angles of 91.16(4) and 92.15(4)° with pyrazolone oxygens translocated in the slightly distorted octahedral geometry. The two EtOH solvent molecules (disordered) are cis located with O5-Ni-O6 bond angle of 89.90(5)° as well as the oxygen donors O1 and O3 of HLV^{III} ligand with O1-Ni-O3 bond angle of 88.19(5)°. In complex-**10,** a HL^{IV} ligand chelates the metal with angles of 89.45(5) and 90.96(5)° but differently from what was observed in complex-**9**, pyrazolone oxygens are here cis located with O1-Ni-O3 bond angle of 91.45(5)°, while O2-Ni-O4 bond angle is of 174.25(5)°. The bond angle O5-Ni-O1w between DMF and the water oxygen atoms is 87.88(5)°. The geometry of centrosymmetric complex-**11** has HL^{VI} chelating ligands in the equatorial plane of the octahedral geometry, while the DMSO molecules occupy the axial positions. The chelating bond angle O1-Ni-O2 is 91.15(6)°. Data of bond angles in **Table 5.13.** gives an indication of the distortions in the octahedral

geometry in each case. **Table 5.10.** represents the bond lengths and bond angles parameters of all three complexes. The hydrogen bond parameters and symmetry transformations of complexes **9, 10** and **11** are presented in **Tables 5.6-5.11.** The symmetry elements present in **complex-11** are shown in **Fig.5.18.** A **Fig.5.19.** Presents 2D representations of the single crystal structures of complexes **9, 10,** and **11.**

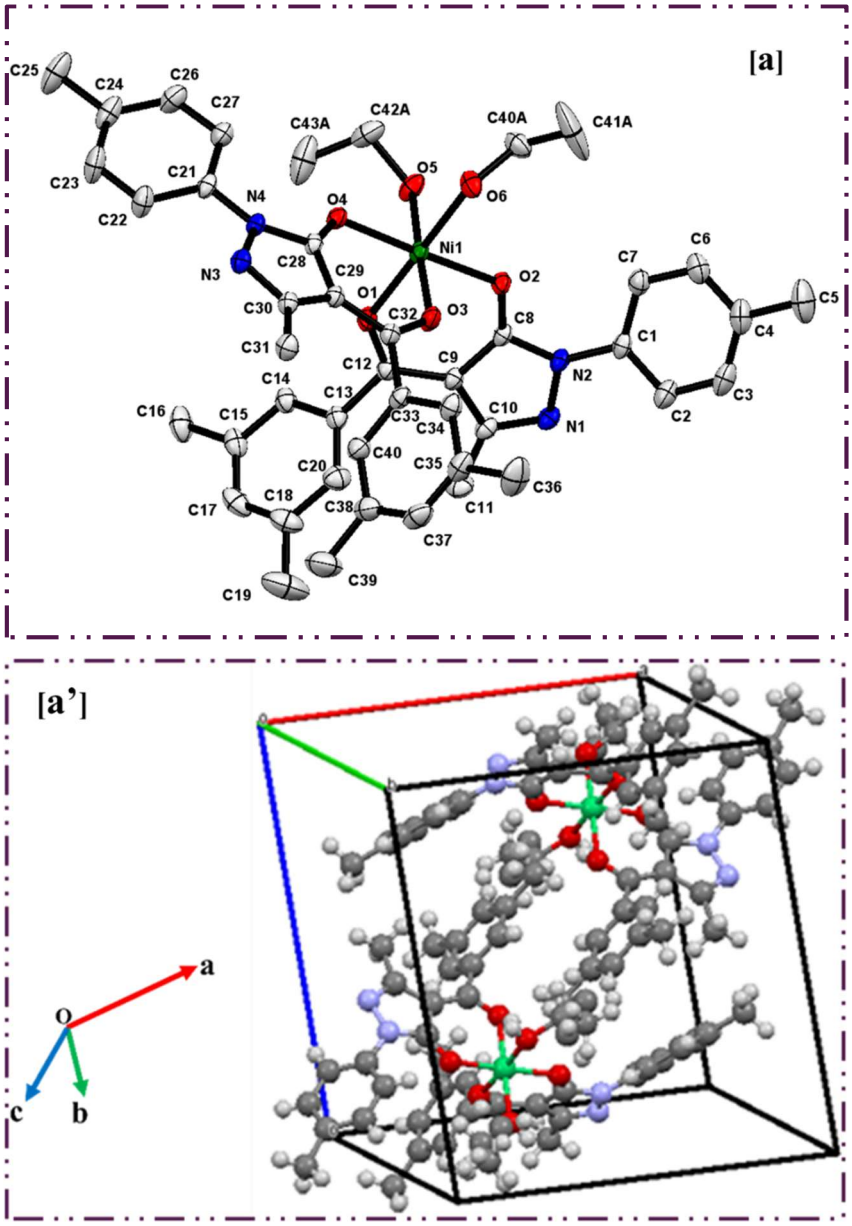

Fig.5.15. (a)= Molecular structure of complex-9 with anisotropic displacement ellipsoids drawn at 40 % with only each one position of disordered EtOH shown (Hydrogen atoms omitted for clarity) and (a')= A perspective view of crystal packing plot of complex-9

Table 5.6. Hydrogen bond parameters of complex-9

D-H...A	d(D-H)	d(H...A)	d(D...A)	<(DHA)
O(5)-H(5AA)-N(1)	0.853(9)	2.018(13)	2.8511(17)	165(4)
C(42B)-H(42D)-O(4)	0.97	2.38	3.062(8)	127.1
O(6)-H(6A)-N(3)	0.833(15)	1.971(16)	2.8041(16)	178(2)

Table 5.7. Complex-9: Symmetry transformation used to generate equivalent atoms

	Symmetry transformations
1	x, y, z
2	-x, -y, -z

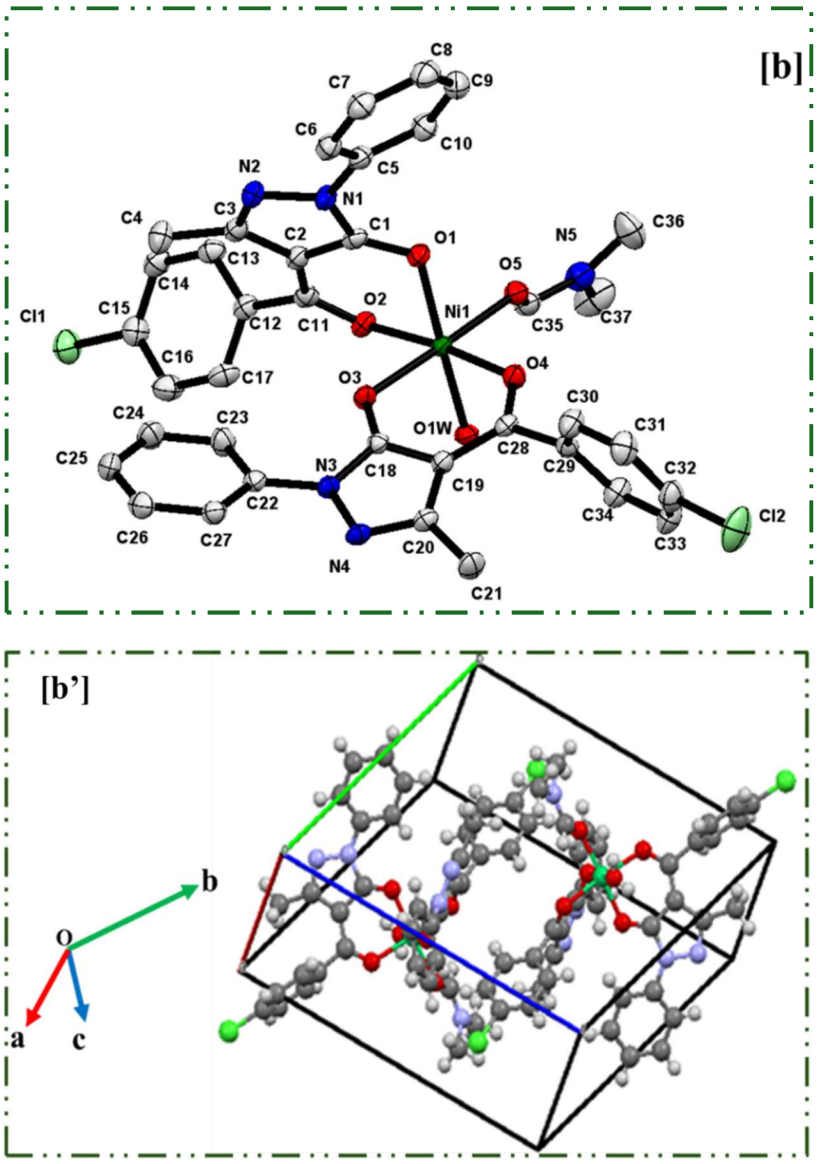

Fig.5.16. (b)= Molecular structure of complex-10 with anisotropic displacement ellipsoids drawn at 50% (Hydrogen atoms omitted for clarity) and (b')= A perspective view of crystal packing plot of complex-10

Table 5.8. Hydrogen bond parameters of complex-10

D-H...A	d(D-H)	d(H...A)	d(D...A)	<(DHA)
O(1W)-H(1W1)-N(2)#1	0.805(16)	2.071(18)	2.8532(19)	164(3)
O(1W)-H(1W2)-N(4)#2	0.792(16)	2.000(17)	2.7793(18)	168(3)
C(10)-H(10A)-O(1)	0.95	2.53	3.006(2)	110.9
C(14)-H(14A)-O(1)#3	0.95	2.65	3.239(2)	120.8
C(14)-H(14A)-O(5)#3	0.95	2.64	3.361(2)	133.4
C(21)-H(21B)-Cl(2)#4	0.98	2.97	3.852(2)	150.5
C(23)-H(23A)-O(3)	0.95	2.26	2.867(2)	121.3
C(33)-H(33A)-Cl(1)#5	0.95	2.98	3.5846(19)	122.6

Table 5.9. Complex-10: Symmetry transformation used to generate equivalent atoms

	Symmetry transformations
1	x+1,y,z
2	-x+2,-y+1,-z
3	-x+1,-y+1,-z+1
4	-x+2,-y,-z
5	x+1,y-1,z

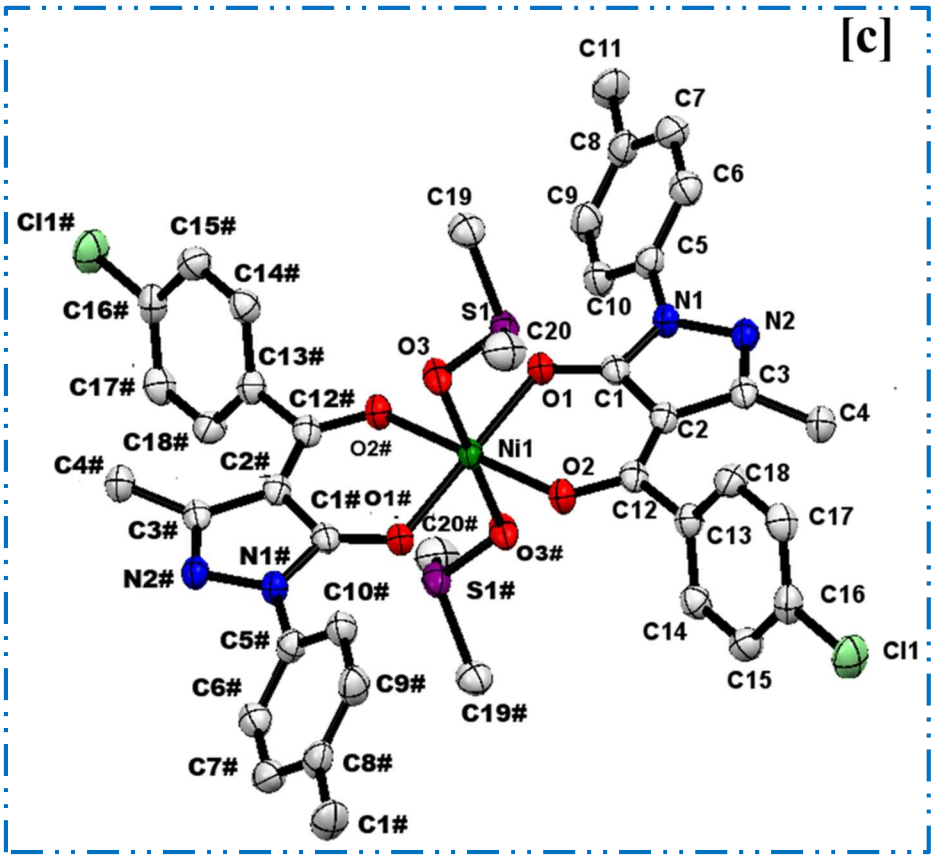

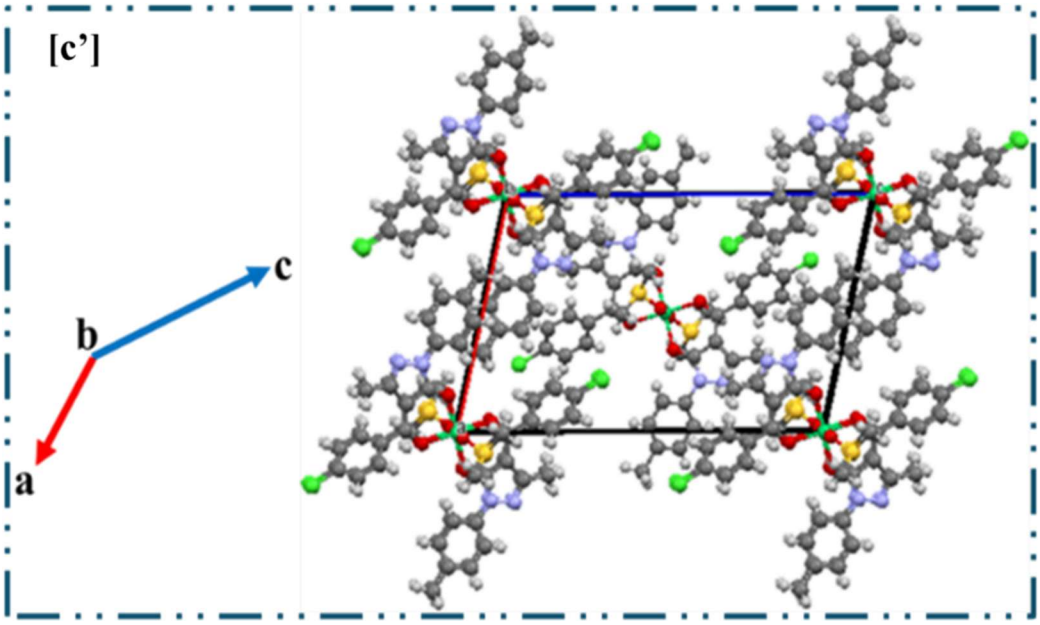

Fig.5.17. (c)= Molecular structure of complex-3 with anisotropic displacement ellipsoids drawn at 50% (Hydrogen atoms omitted for clarity) and (c')= A perspective view of crystal packing plot of complex-11

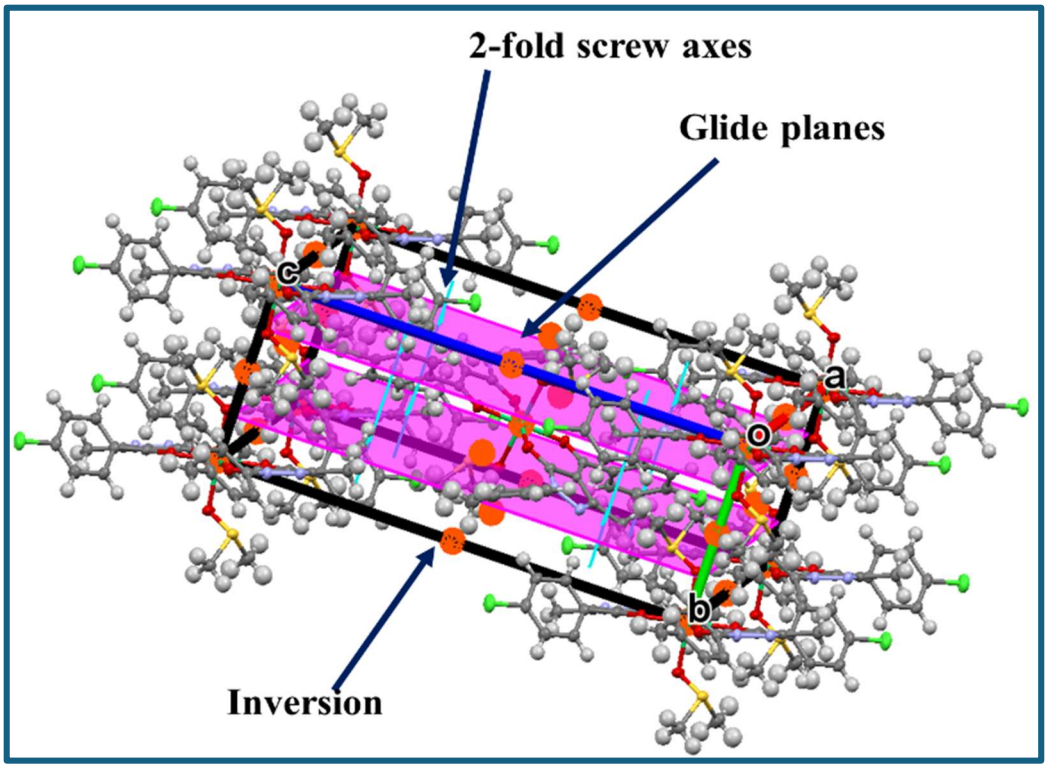

Fig.5.18. Symmetry elements present in complex-11

Table 5.10. Hydrogen bond parameters of complex-11

D-H...A	d(D-H)	d(H...A)	d(D...A)	<(DHA)
C(4)-H(4A)-S(1)#2	0.98	3.00	3.648(2)	124.9
C(19)-H(19C)-O(3)#3	0.98	2.42	3.353(3)	159.5
C(20)-H(20A)-Cl(1)#4	0.98	2.81	3.713(3)	154.2

Table 5.11. Complex-11: Symmetry transformation used to generate equivalent atoms

	Symmetry transformations
1	-x+1,-y+1,-z+1
2	-x+3/2,y-1/2,-z+3/2
3	-x+1,-y+2,-z+1
4	-x+1/2,y+1/2,-z+3/2

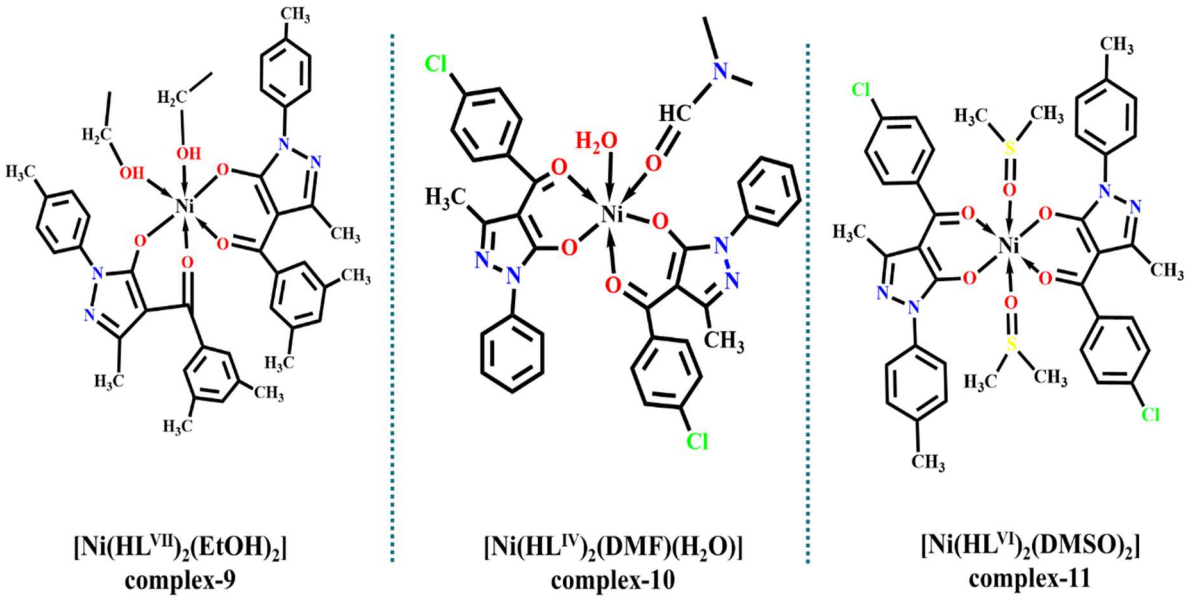

Fig.5.19. 2D representation of the single crystal structures of complex-9, complex-10 and complex-11

Table 5.12. Crystal data and details of refinement of Nickel Complexes

CODE	$[Ni(HL^{VIII})_2(EtOH)_2]$ Complex-9	$[Ni(HL^{IV})_2(DMF)(H_2O)]$ Complex-10	$[Ni(HL^{VI})_2(DMSO)_2]$ Complex-11
CCDC number	2304477	2304476	2304475
Chemical formula	$C_{44}H_{50}N_4NiO_6$	$C_{37}H_{33}Cl_2N_5NiO_6$	$C_{40}H_{40}Cl_2N_4NiO_6S_2$
Formula weight	789.59	773.29	866.49
Crystal system	Triclinic	Triclinic	Monoclinic
Space group	*P*-1	*P*-1	$P2_1/n$
Temperature	298(2) K	100(2) K	100(2) K
Wavelength	1.54178 Å	1.54184 Å	1.54184 Å
Z	2	2	2
Density	1.278 Mg/m^3	1.540 Mg/m^3	1.458 Mg/m^3
Unit cell dimension	a= 13.09000(10) Å, b= 13.52230(10) Å c= 14.4319(2) Å	a = 9.3204(2) Å b = 13.4575(3) Å c = 15.0835(4) Å	a= 12.7053(2) Å b= 7.7512(1) Å c= 20.5913(4) Å
	α= 64.8740(10)° β= 85.4660(10)° γ= 63.5340(10)°	α= 65.196(2)° β= 76.269(2)° γ= 84.907(2)°	α= 90° β= 103.215(2)° γ= 90°
F (0 0 0)	836	800	990
Theta range	3.414 to 66.792°	3.310 to 78.871°	3.746 to 78.624°
R(int)	0.0299	0.0328	0.0622
Refined parameters	542	472	254
Absorption Correction	Multi-scan	Semi-empirical from equivalents	Multi-scan
Index ranges	-15<=h<=14, -16<=k<=16, -17<=l<=17	-16<=h<=15, -9<=k<=5, -25<=l<=24	-16<=h<=15, -9<=k<=5, -25<=l<=24
Reflections collected	42254	25055	25055
Goodness-of-fit on F^2	1.058	1.078	1.078
R indices	R1 = 0.0371, wR2 = 0.0928	R1 = 0.0430, wR2 = 0.0926	R1 = 0.0500, wR2 = 0.1235
Min/max electron density	0.184/-0.284	0.453/-0.503	0.562/-0.397

Table 5.13. Bond Lengths and Bond Angles Parameters of Ni(II) complexes

Atoms	Bond lengths	Atoms	Bond angles
Complex-9			
Ni(1)-O(1)	2.0304(11)	O(1)-Ni(1)-O(3)	88.19(5)
Ni(1)-O(2)	2.0054(10)	O(1)-Ni(1)-O(5)	90.73(6)
Ni(1)-O(3)	2.0416(12)	O(1)-Ni(1)-O(6)	178.94(5)
Ni(1)-O(4)	2.0224(10)	O(2)-Ni(1)-O(1)	91.16(4)
Ni(1)-O(5)	2.0933(12)	O(2)-Ni(1)-O(3)	89.36(4)
Ni(1)-O(6)	2.0781(11)	O(2)-Ni(1)-O(4)	178.19(4)
		O(2)-Ni(1)-O(5)	87.06(5)
		O(2)-Ni(1)-O(6)	89.72(4)
		O(3)-Ni(1)-O(5)	176.25(4)
		O(3)-Ni(1)-O(6)	91.23(5)
		O(4)-Ni(1)-O(1)	89.87(4)
		O(4)-Ni(1)-O(3)	92.15(4)
		O(4)-Ni(1)-O(5)	91.44(4)
		O(4)-Ni(1)-O(6)	89.26(4)
		O(6)-Ni(1)-O(5)	89.90(5)
Complex-10			
Ni(1)-O(3)	2.0167(12)	O(3)-Ni(1)-O(1)	91.45(5)
Ni(1)-O(1)	2.0358(12)	O(3)-Ni(1)-O(5)	176.94(5)
Ni(1)-O(5)	2.0595(12)	O(1)-Ni(1)-O(5)	88.99(5)
Ni(1)-O(1W)	2.0737(12)	O(3)-Ni(1)-O(1W)	91.56(5)
Ni(1)-O(4)	2.0741(12)	O(1)-Ni(1)-O(1W)	176.32(5)
Ni(1)-O(2)	2.0761(12)	O(5)-Ni(1)-O(1W)	87.88(5)
		O(3)-Ni(1)-O(4)	90.96(5)
		O(1)-Ni(1)-O(4)	93.43(5)
		O(5)-Ni(1)-O(4)	92.04(5)
		O(1W)-Ni(1)-O(4)	88.64(5)
		O(3)-Ni(1)-O(2)	83.98(5)
		O(1)-Ni(1)-O(2)	89.45(5)
		O(5)-Ni(1)-O(2)	93.00(5)
		O(1W)-Ni(1)-O(2)	88.76(5)
		O(4)-Ni(1)-O(2)	174.25(5)
Complex-11			
Ni(1)-O(1)	2.0340(15)	O(1)-Ni(1)-O(1)#1	180.0
Ni(1)-O(1)#1	2.0340(15)	O(1)-Ni(1)-O(2)	91.15(6)
Ni(1)-O(2)	2.0491(15)	O(1)#1-Ni(1)-O(2)	88.85(6)
Ni(1)-O(2)#1	2.0491(15)	O(1)-Ni(1)-O(2)#1	88.85(6)
Ni(1)-O(3)#1	2.0884(15)	O(1)#1-Ni(1)-O(2)#1	91.15(6)
Ni(1)-O(3)	2.0884(15)	O(2)-Ni(1)-O(2)#1	180.0
		O(1)-Ni(1)-O(3)#1	89.77(6)
		O(1)#1-Ni(1)-O(3)#1	90.23(6)
		O(2)-Ni(1)-O(3)#1	89.05(6)
		O(2)#1-Ni(1)-O(3)#1	90.95(6)
		O(1)-Ni(1)-O(3)	90.23(6)
		O(1)#1-Ni(1)-O(3)	89.77(6)
		O(2)-Ni(1)-O(3)	90.95(6)
		O(2)#1-Ni(1)-O(3)	89.05(6)
		O(3)#1-Ni(1)-O(3)	180.0

5.3.7 Powder XRD study

Pale bluish-green, pale-green and pale-yellow green x-ray grade crystals of three Nickel(II) complexes were formed using a slow evaporation technique. Powder XRD is regarded as a method for bulk characterization. Phase identification of crystalline materials is accomplished by X-ray powder diffraction (XRD), a quick analytical method. It can also provide details on the size of unit cells. The subject matter is homogenized coarsely powdered, and the average composition of the material is identified. Thus, from the single crystal data, a simulated pattern for both complexes were obtained, and the powder XRD experiment lined up with the experimental pattern. There is enough similarity between the characteristics of all three Ni(II) complexes; hence, there is no point in attempting the said analysis for individual fits. Thus, Powder XRD analysis was done for complex-**10** and complex-**11**. This proves that bulk products are the same as those in single-crystal form. This further shows that each complex has the same geometry and composition. This implies that many complexes are well-represented by the single crystal from which the structure was formed. The XRD graph displays a distinct band with peaks 2θ = 5 to 20° range for the complex-**10** and 2θ = 5 to 25° range for the complex-**11**. The simulated and powder XRD patterns of complex-**10** and complex-**11** are displayed in **Figs.5.20-5.21,** respectively.

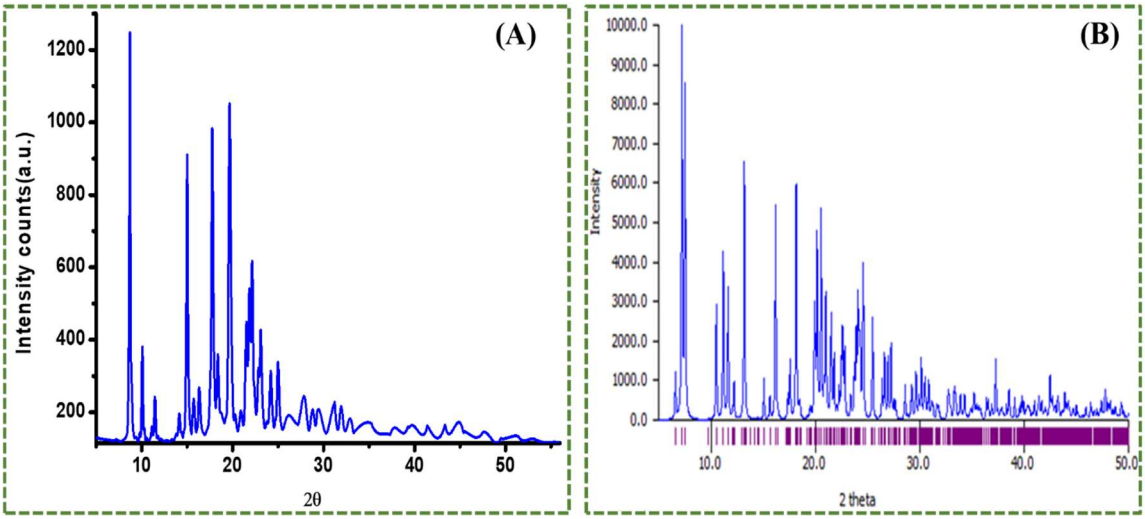

Fig.5.20. Comparison of the powder XRD patterns for complex-10 in (A) the experimental and (B) the simulated

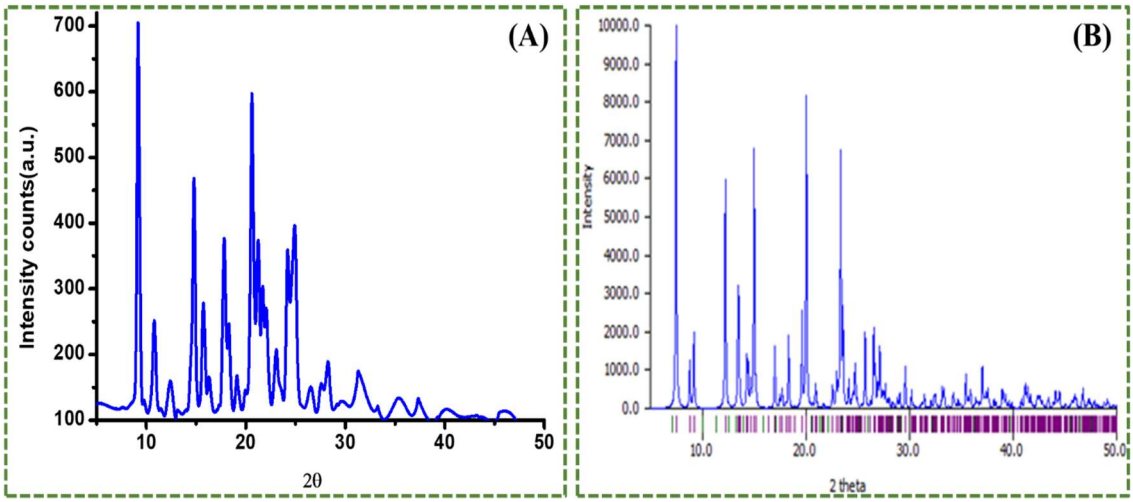

Fig.5.21. Comparison of the powder XRD patterns for complex-11 in (A) the experimental and (B) the simulated conditions

5.3.8 Computational analysis of compounds employing DFT study

An isolated molecule was used for the theoretical calculations, while an experimental result was determined in a solid state [28]. DFT computations and geometrical optimization of three Ni(II) complexes were carried out using the B3LYP approach and Gaussview 6.0 was used for the processing of the input files [29][30]. Using an effective core potential for Ni, the LanL2DZ basis set was employed [31]. The optimization energies` of complex-**9**, complex-**10** and complex-**11** are -105.7622 keV, -64.0523 keV and -66.3350 keV, respectively. More negative optimization energy value of complex-**9** suggests greater stability. Many chemical interactions are determined by the HOMO-LUMO energies**.** In addition to indicating chemical stability, HOMO-LUMO orbitals are essential for figuring out a molecule's electrical transport properties [28]**.** Ultimately, the octahedral geometry of each complex is confirmed by the DFT computations [32]. The HOMO-LUMO energy values of all three complexes are displayed in **Table 5.14.** The global parameters of complex-**9**, complex-**10** and complex-**11** are displayed in **Tables 5.15-5.17,** respectively. **Figs. 5.22-5.24** show the DFT-optimized geometries and the HOMO-LUMO molecular orbital diagrams of complex-**9**, complex-**10**, and complex-**11**, respectively. By comparing the bond angles and distances between the DFT-optimized and X-ray-determined structures of complexes, the structural agreement has been confirmed. Since the experimental data were obtained in a solid state, while the theoretical calculations were conducted on isolated molecular components in the gas phase, the optimized bond lengths and angles are somewhat larger than the experimental ones, and even theoretical IR frequencies are higher than the practical FT-IR frequencies which are mentioned in **Tables 5.1-5.3. (Section 5.3.1.).** Hence, the optimized geometry is in

good agreement with the experimental data. A comparison of the practical and theoretical bond parameters of all three complexes is mentioned in **Table 5.18.**

5.3.8.1 A Frontier molecular orbital energy (HOMO-LUMO) analysis

Frontier molecular orbital energy (HOMO-LUMO) is calculated via the B3LYP/LANL2DZ level basis set. Molecular orbitals often provide information about the kind of reactivity, conjugation, lone pairs, and certain physical characteristics of reacting species. HOMO and LUMO energies are used to characterise the ability to donate and take electrons, respectively. At the same time, the Chemical stability and electrical transport properties of molecules are expressed in terms of energy gap (ΔE) [33]. The stability of the molecular bond is shown via the difference in energy between the LUMO and HOMO orbitals. A stable molecule with low chemical reactivity is indicated by a high HOMO-LUMO gap. To ascertain the electrical transport characteristics of molecules, the HOMO-LUMO difference is important [28]. The energy gap (ΔE) values are 3.800 eV, 2.998 eV and 3.299 eV for complexes **9, 10** and **11,** respectively. **Complex-10** is more reactive due to its lower ΔE value. The stability order of complexes is,

Complex-9 > Complex-11 > Complex-10

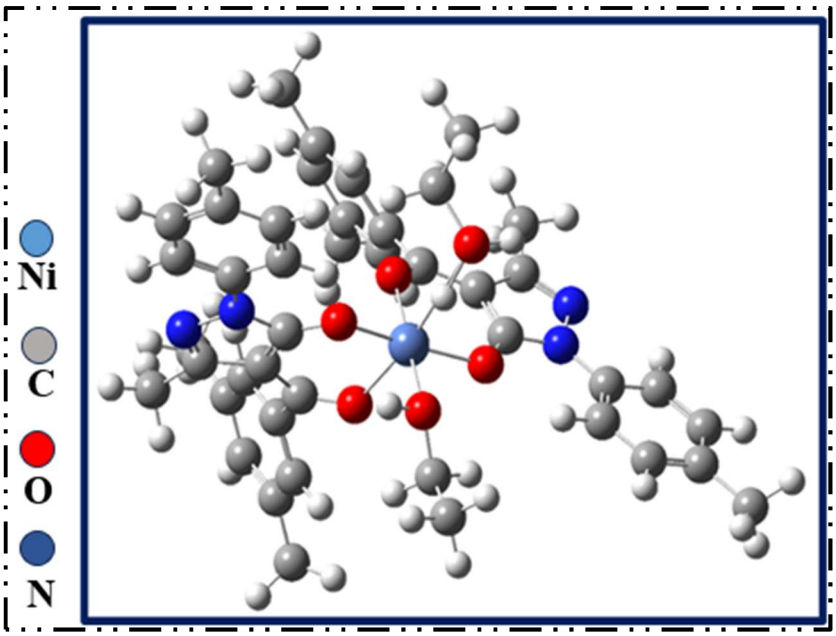

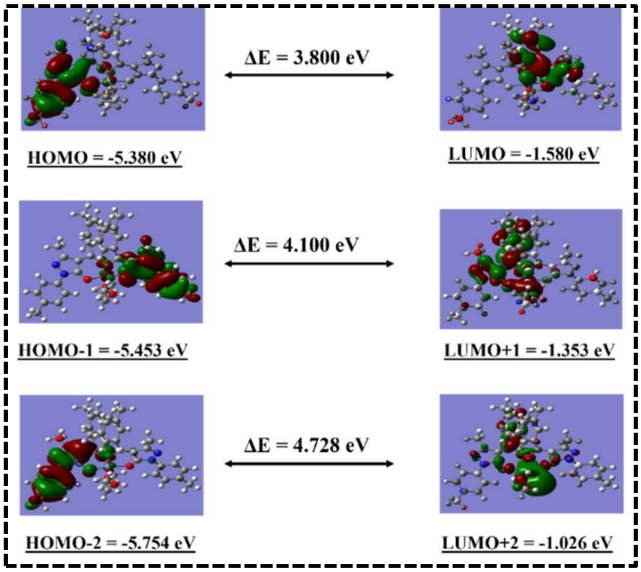

Fig.5.22. Complex-9: DFT optimized Structure and HOMO-LUMO molecular diagram

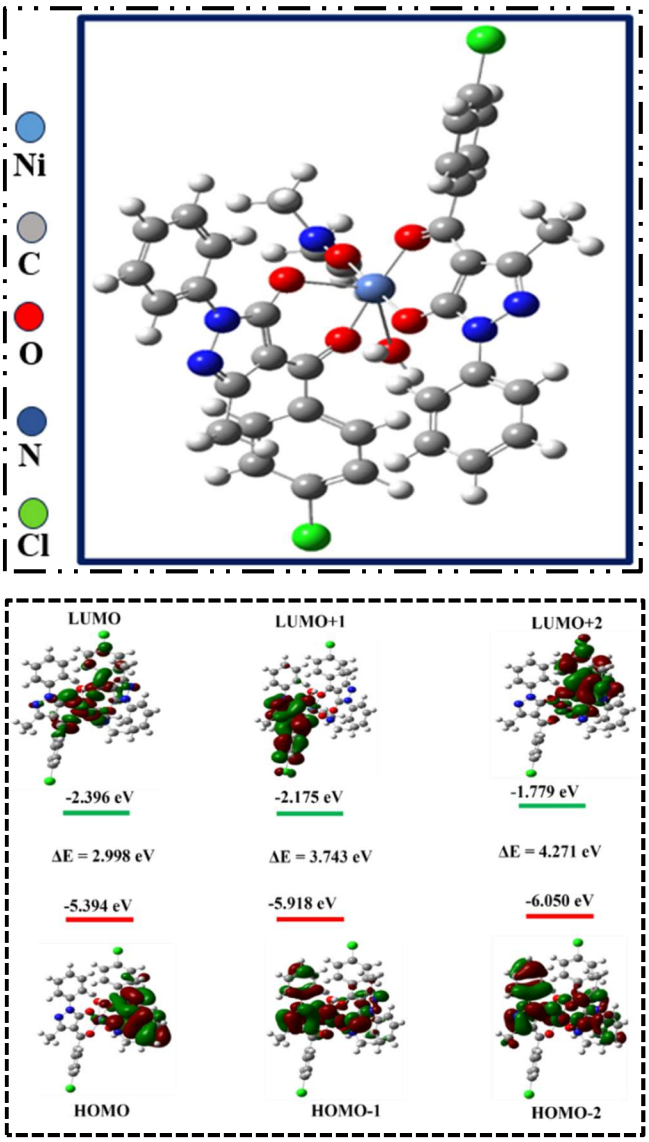

Fig.5.23. Complex-10: DFT optimized Structure and HOMO-LUMO molecular diagram

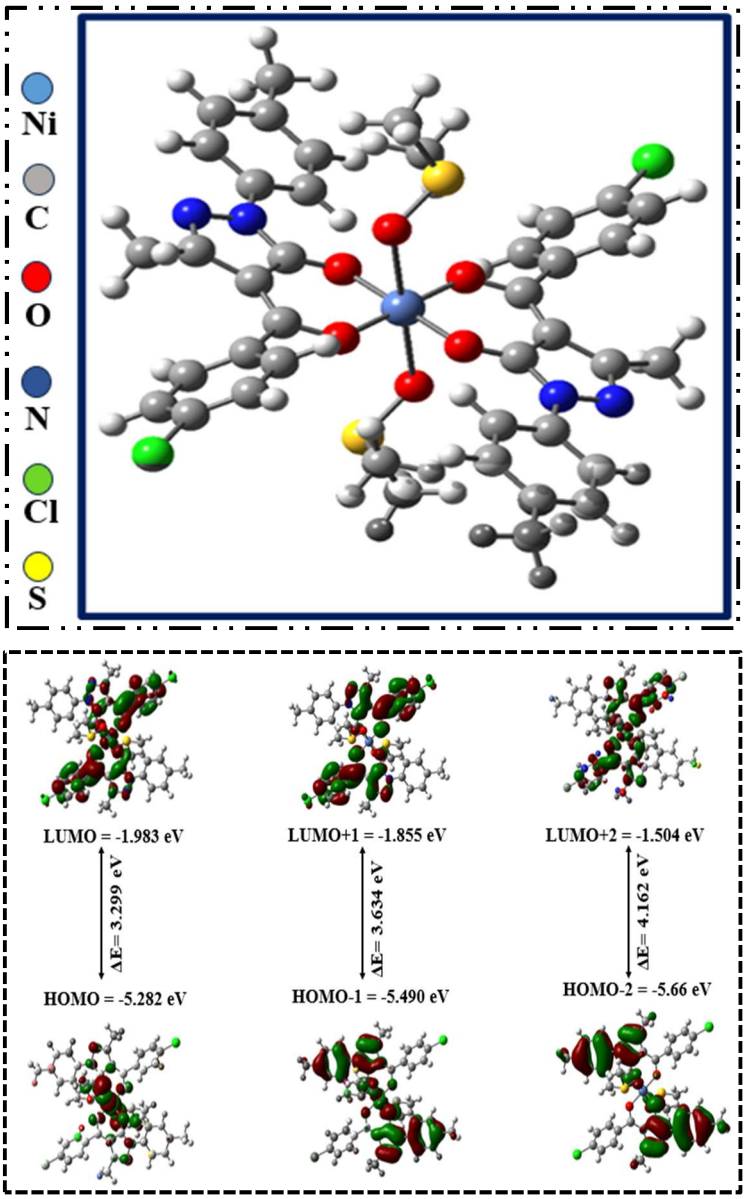

Fig.5.24. Complex-11: DFT optimized Structure and HOMO-LUMO molecular diagram

Table 5.14. HOMO-LUMO energy values complex-9, complex-10 and complex-11

Levels	Molecular orbital energy (eV)		
	Complex-9	Complex-10	Complex-11
	LANL2DZ	LANL2DZ	LANL2DZ
HOMO	-5.380	-5.394	-5.282
LUMO	-1.580	-2.396	-1.983
HOMO-1	-5.453	-5.918	-5.490
LUMO+1	-1.353	-2.175	-1.855
HOMO-2	-5.754	-6.050	-5.667
LUMO+2	-1.026	-1.779	-1.504

Table 5.15. Global parameters of complex-9

Properties	Mathematical Formula	Complex-9
E_{HOMO}	E_{HOMO}	-5.380
E_{LUMO}	E_{LUMO}	-1.580
ΔE	$\Delta E = E_{LUMO} - E_{HOMO}$	3.800
Ionization potential (IP)	$IP = -E_{HOMO}$	5.380
Chemical Potential (μ)	$\mu = 1/2 (E_{HOMO} + E_{LUMO})$	-3.480
Electron affinity (EA)	$EA = -E_{LUMO}$	1.580
Electronegativity (EN)	$EN = -1/2 (E_{HOMO} + E_{LUMO})$	3.480
Global Hardness (Ƞ)	$\eta = -1/2 (E_{HOMO} - E_{LUMO})$	1.900
Softness (S)	$S = 1/2\eta$	0.263
Electrophilicity index (ω)	$\omega = \mu^2/2\eta$	3.187

Table 5.16. Global parameters of complex-10

Properties	Mathematical Formula	Complex-10
E_{HOMO}	E_{HOMO}	-5.394
E_{LUMO}	E_{LUMO}	-2.396
ΔE	$\Delta E = E_{LUMO} - E_{HOMO}$	2.998
Ionization potential (IP)	$IP = -E_{HOMO}$	5.394
Chemical Potential (μ)	$\mu = 1/2 (E_{HOMO} + E_{LUMO})$	-3.895
Electron affinity (EA)	$EA = -E_{LUMO}$	2.396
Electronegativity (EN)	$EN = -1/2 (E_{HOMO} + E_{LUMO})$	3.895
Global Hardness (Ƞ)	$\eta = -1/2 (E_{HOMO} - E_{LUMO})$	1.499
Softness (S)	$S = 1/2\eta$	0.333
Electrophilicity index (ω)	$\omega = \mu^2/2\eta$	5.060

Table 5.17. Global parameters of complex-11

Properties	Mathematical Formula	Complex-11
E_{HOMO}	E_{HOMO}	-5.282
E_{LUMO}	E_{LUMO}	-1.983
ΔE	$\Delta E = E_{LUMO} - E_{HOMO}$	3.299
Ionization potential (IP)	$IP = -E_{HOMO}$	5.282
Chemical Potential (μ)	$\mu = 1/2 (E_{HOMO} + E_{LUMO})$	-3.632
Electron affinity (EA)	$EA = -E_{LUMO}$	1.983
Electronegativity (EN)	$EN = -1/2 (E_{HOMO} + E_{LUMO})$	3.632
Global Hardness (Ƞ)	$\eta = -1/2 (E_{HOMO} - E_{LUMO})$	1.649
Softness (S)	$S = 1/2\eta$	0.303
Electrophilicity index (ω)	$\omega = \mu^2/2\eta$	3.999

Table 5.18. A comparison of the practical and theoretical bond parameters

Atoms	Practical bond length (Å)	Theoretical bond length (Å)	Atoms	Practical bond angles (°)	Theoretical bond angles (°)
Complex-9					
Ni(1)-O(1)	2.0304(11)	2.065	O(1)-Ni(1)-O(3)	88.19(5)	91.35
Ni(1)-O(2)	2.0054(10)	2.036	O(1)-Ni(1)-O(5)	90.73(6)	95.24
Ni(1)-O(3)	2.0416(11)	2.056	O(1)-Ni(1)-O(6)	178.94(5)	180.42
Ni(1)-O(4)	2.0224(11)	2.098	O(2)-Ni(1)-O(1)	91.16(4)	95.50
Ni(1)-O(5)	2.0933(12)	2.167	O(2)-Ni(1)-O(6)	89.72(4)	90.70
Ni(1)-O(6)	2.0781(11)	2.145	O(4)-Ni(1)-O(3)	92.15(4)	96.56
Complex-10					
Ni(1)-O(3)	2.0167(12)	2.020	O(3)-Ni(1)-O(1)	91.45(2)	92.45
Ni(1)-O(1)	2.0358(12)	2.041	O(3)-Ni(1)-O(5)	176.94(5)	180.91
Ni(1)-O(5)	2.0595(12)	2.165	O(1)-Ni(1)-O(5)	88.99(5)	90.34
Ni(1)-O(1W)	2.0737(12)	2.231	O(3)-Ni(1)-O(4)	90.96(5)	92.68
Ni(1)-O(4)	2.0741(12)	2.145	O(1)-Ni(1)-O(4)	93.43(5)	95.67
Ni(1)-O(2)	2.0761(12)	2.178	O(5)-Ni(1)-O(2)	93.00(5)	95.87
Complex-11					
Ni(1)-O(1)	2.0340(15)	2.040	O(1)-Ni(1)-O(1)#1	180.0	180.70
Ni(1)-O(1)#1	2.0340(15)	2.039	O(1)-Ni(1)-O(2)	91.15(6)	92.20
Ni(1)-O(2)	2.0491(15)	2.153	O(1)#1-Ni(1)-O(2)	88.85(6)	90.35
Ni(1)-O(2)#1	2.0491(15)	2.117	O(1)-Ni(1)-O(2)#1	88.85(6)	90.30
Ni(1)-O(3)#1	2.0884(15)	2.146	O(1)#1-Ni(1)-O(2)#1	91.15(6)	93.15
Ni(1)-O(3)	2.0884(15)	2.189	O(2)-Ni(1)-O(2)#1	180.0	180.81

5.3.8.2 Natural bond orbital (NBO) analysis

Measurable donor-acceptor stabilising interactions occur between occupied Lewis-type NBOs (donor) and unoccupied non-Lewis-type NBOs (acceptor/Reydberg). This interaction is linked to the delocalization of electron density. Utilizing a LANL2DZ basis set and the B3LYP approach, the natural bond orbital (NBOs) analysis of the linked complexes has been examined. It is believed that coordination bonds involving oxygen atoms underlie any exchanges between a donor atom and a Ni(II) ion. An electron density has been transferred due to this interaction from the acylpyarazolone ligand's donor atom, LP(O), to the antibonding orbital of LP*(Ni). In complex-**9** the natural atomic charge on Ni^{+2} is 0.8878. The native electronic configuration of nickel is [core] 3d (8.52) 4s (0.24) 4p (0.14). The valence electrons (9.1087), core electrons (17.9937) and total electrons are 27.1221. In the complex-**10**, the natural atomic charge on Ni^{+2} is 0.8478. The native

electronic configuration of nickel is [core] 3d (8.54) 4s (0.26) 4p (0.11). The valence electrons (9.1487), Core electrons (17.9935) and Total electrons are 27.1521 [34][9]. For complex-11, an observed electronic arrangement is [core] 3d (8.53) 4s (0.265 4p (0.12). Such information from the NBO analysis has proved that Nickel metal ion has a +2 charge in the complex.

5.3.9 2D fingerprint combined with Hirshfeld surface analysis

The Hirshfeld surface was developed as a way to define the region occupied by a molecule within a crystal, with the aim of dividing the crystal's electron density into individual molecular fragments [35]. The evaluation of the Hirshfeld surface was used to visually represent and measure the variations and convergences of intermolecular interactions among the crystal structures. The quantitative ratios of short contacts between atoms allow for the identification of weak hydrogen bond intermolecular interactions, and the locations of these interactions can be determined through this study [36]. The CrystalExplorer software was originally created to support Hirshfeld surface (HS) analysis and this remains one of its main functions [37]. CrystalExplorer17 has been used to make the molecules' 2D fingerprint plots and Hirshfeld surface analysis in this study, which also helped to show the structural links between the structural configurations of these closely related molecules. This shows the hydrogen bonding and interaction by plotting the Hirshfeld surface (HS) using a range of variables, such as normalised distances (dnorm), de, di, form index, curvedness, fragment patch, etc. The detailed explanation and study of this said analysis has already been thoroughly discussed in the previous chapters **(Chap. 2-4).** To enable molecular structure visualisation, Hirshfeld surfaces for dnorm were constructed as transparent surfaces. The major donor-acceptor interactions were shown by red areas on the complexes [38]. When the value of dnorm is negative, it indicates that the intermolecular contacts are shorter than the van der Waals radius. π···π stacking interactions are shown by the HS over the shape index and curvedness that improve the stability of the crystal [39]. **Fig.5.25 (A', A" and A"')** shows the molecular Hirshfeld diagrams for each of the three complexes. **Figs.5.26-5.28** represent the 2D fingerprint plots of complex-**9**, complex-**10** and complex-**11,** respectively.

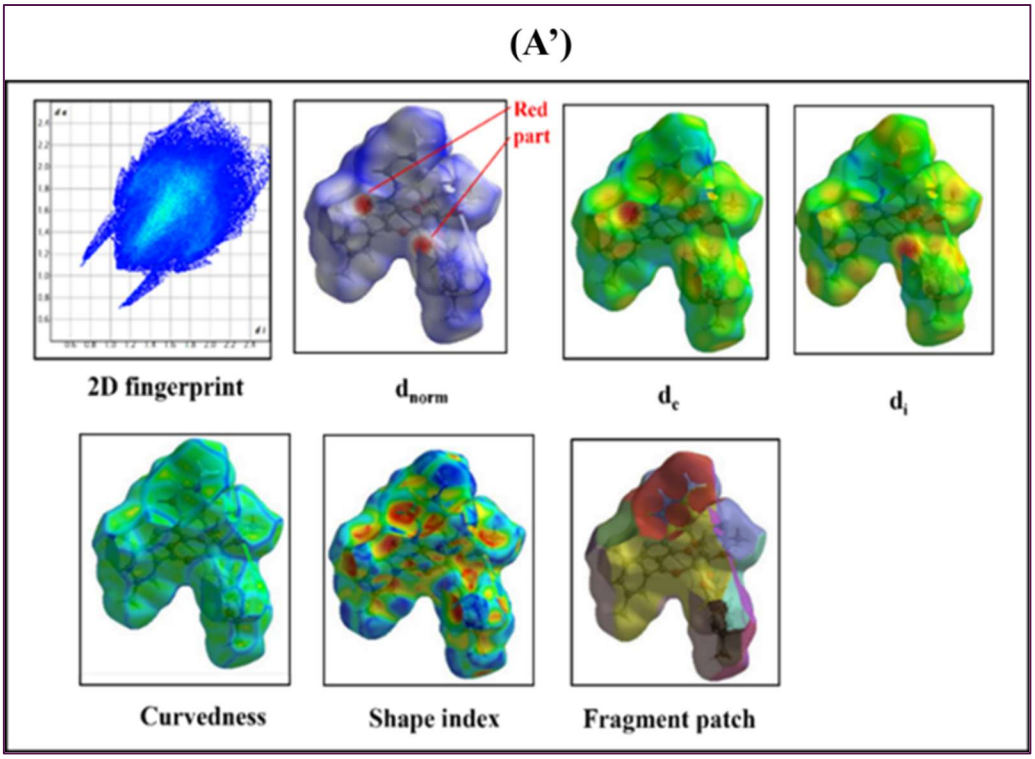
(A')
Red part
2D fingerprint
d_{norm}
d_e
d_i
Curvedness
Shape index
Fragment patch

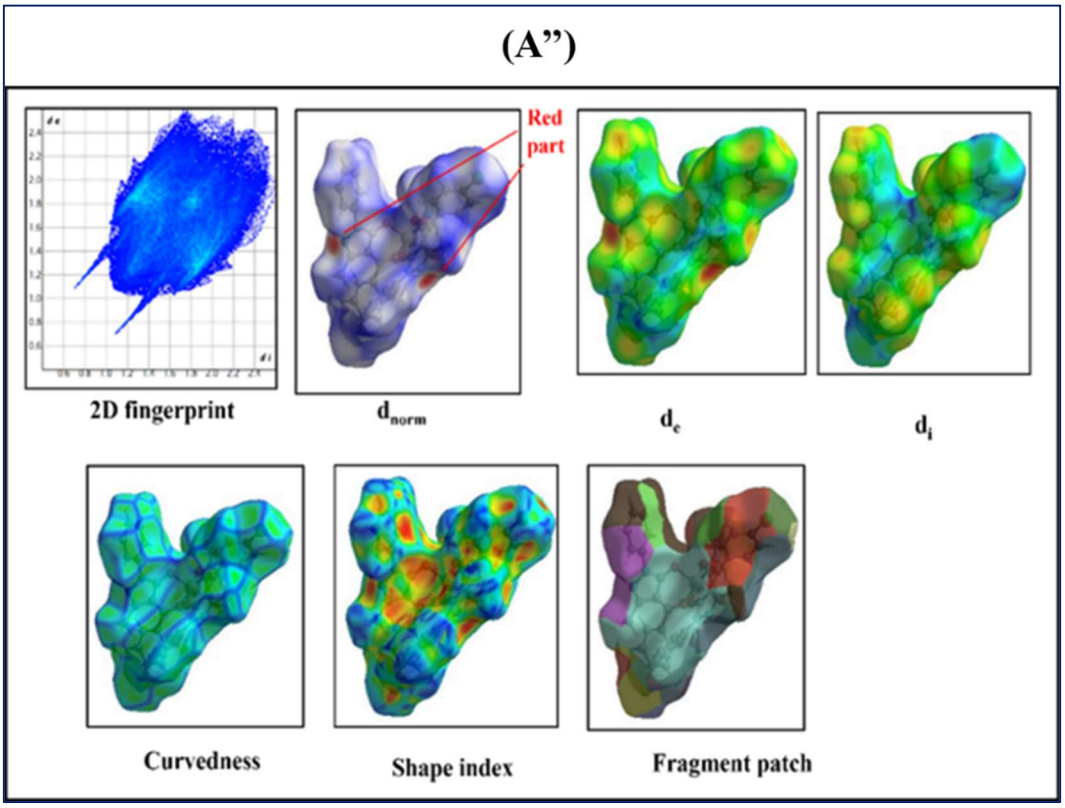
(A")
Red part
2D fingerprint
d_{norm}
d_e
d_i
Curvedness
Shape index
Fragment patch

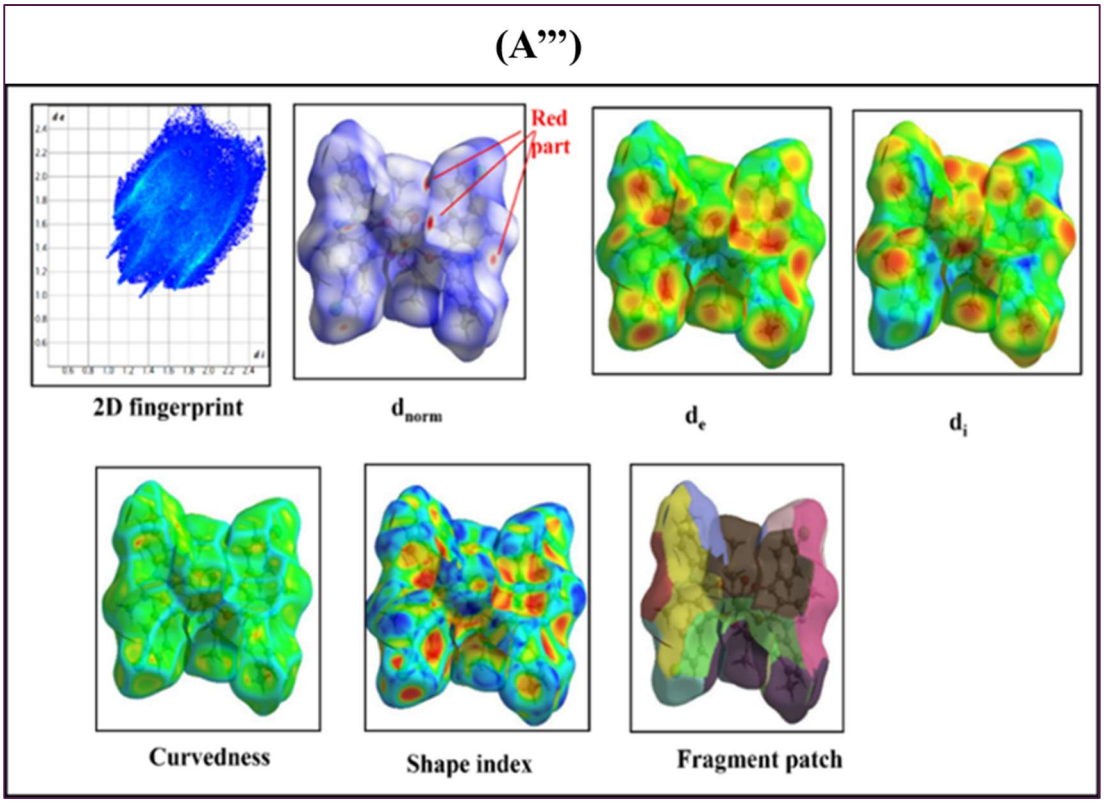

Fig.5.25. The molecular Hirshfield (full FP diagram, dnorm, di, de, Curvedness, Shape index, and fragment patch) (A') complex-9, (A") complex-10, (A"') complex-11

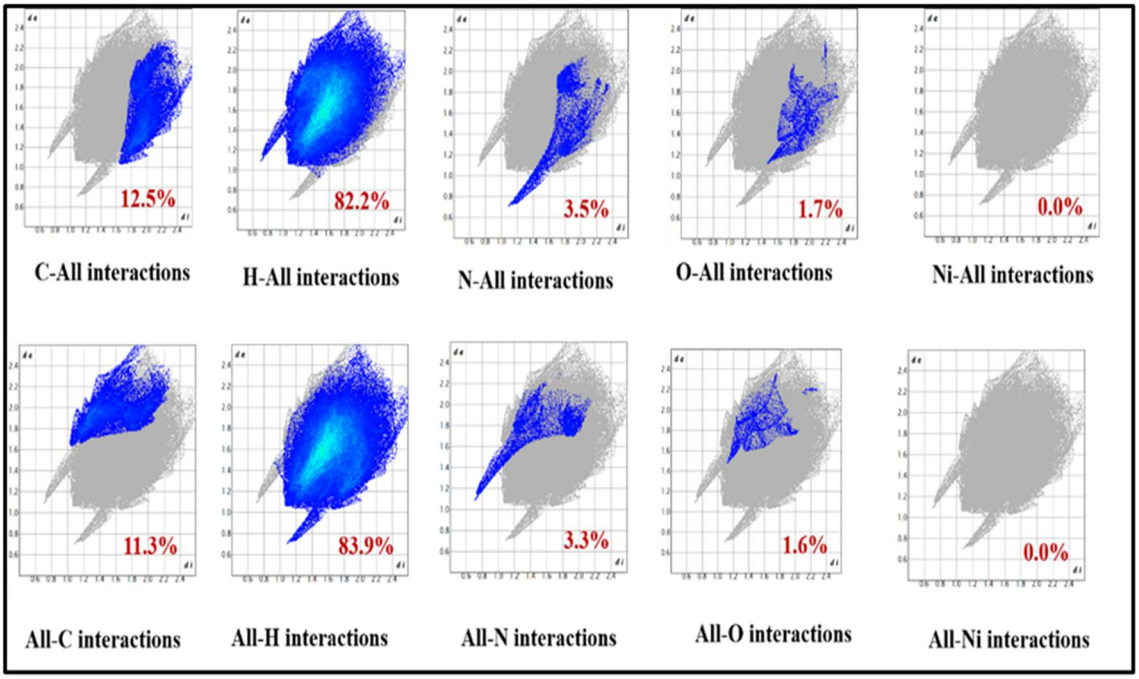

Fig.5.26. Two-dimensional fingerprint plots of complex-9 for atom-all and all-atom interactions

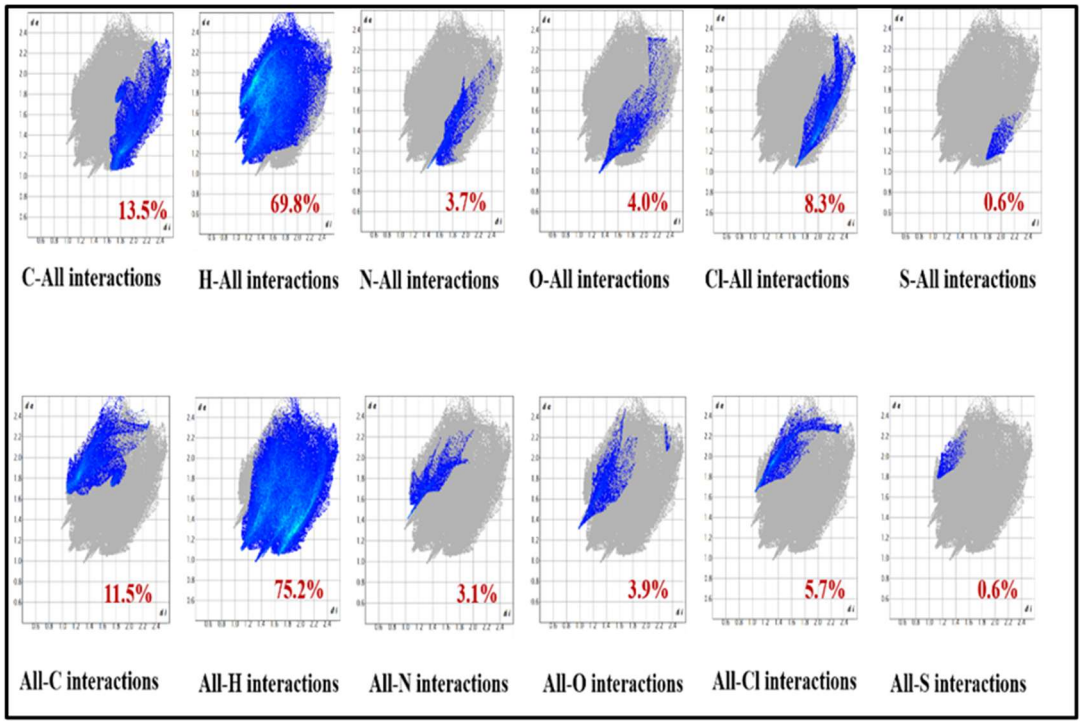

Fig.5.27. Two-dimensional fingerprint plots of complex-10 for atom-all and all-atom interactions

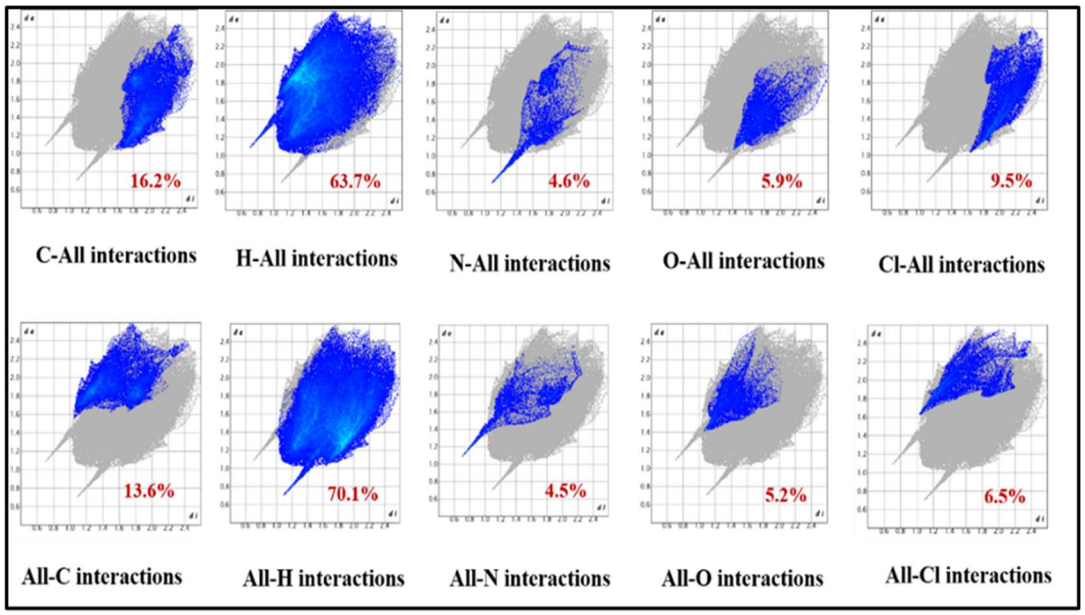

Fig.5.28. Two-dimensional fingerprint plots of complex-11 for atom-all and all-atom interactions

The packing potential of the compound can be assessed by using percentage statistics for interactions between all atoms and specific atoms. This method offers a deeper understanding of how atoms interact with their surrounding environment. Two important concepts in this analysis are ‘atom-to-all’ and ‘all-to-atom’ interactions.

In all the Nickel complexes, there is no interaction between Ni-All and All-Ni, indicating that nickel has no secondary relations among nearby atoms. All the complexes exhibit considerable H interaction. 82%, 70% and 64% H-All in complex-**9**, complex-**10**, and complex-**11,** respectively. While for All-H 42%, 75%, and 70% in complex-**9**, complex-**10**, and complex-**11** respectively. The graphical presentation of the percentage interactions between each inside and outside atom of complexes **9, 10** and **11** are pictured in **Figs.5.29-5.31,** respectively.

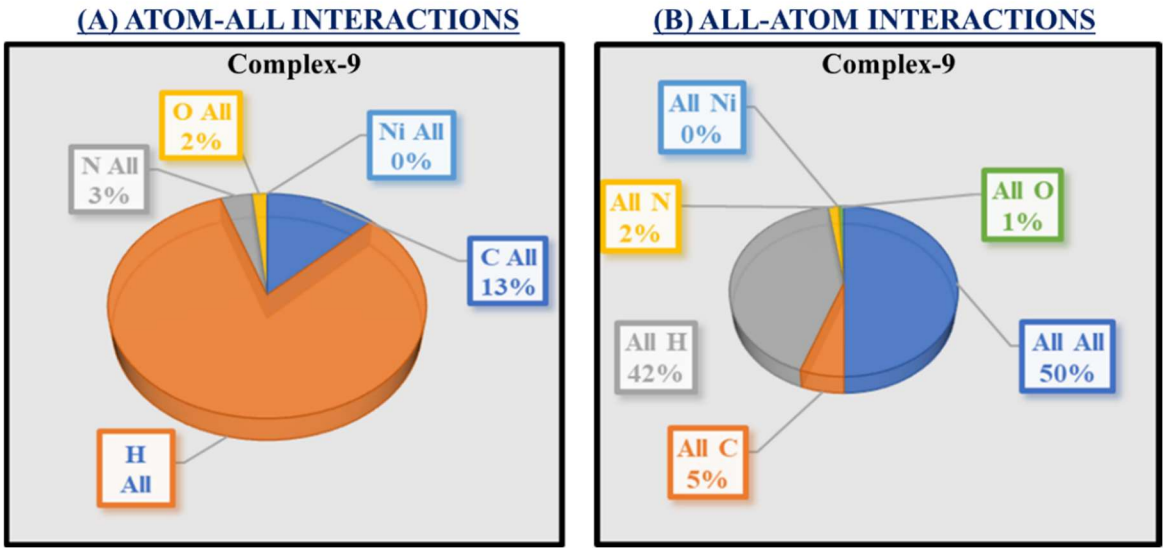

Fig.5.29. Graphical presentation of percentage interactions between each inside and outside atom of complex-9

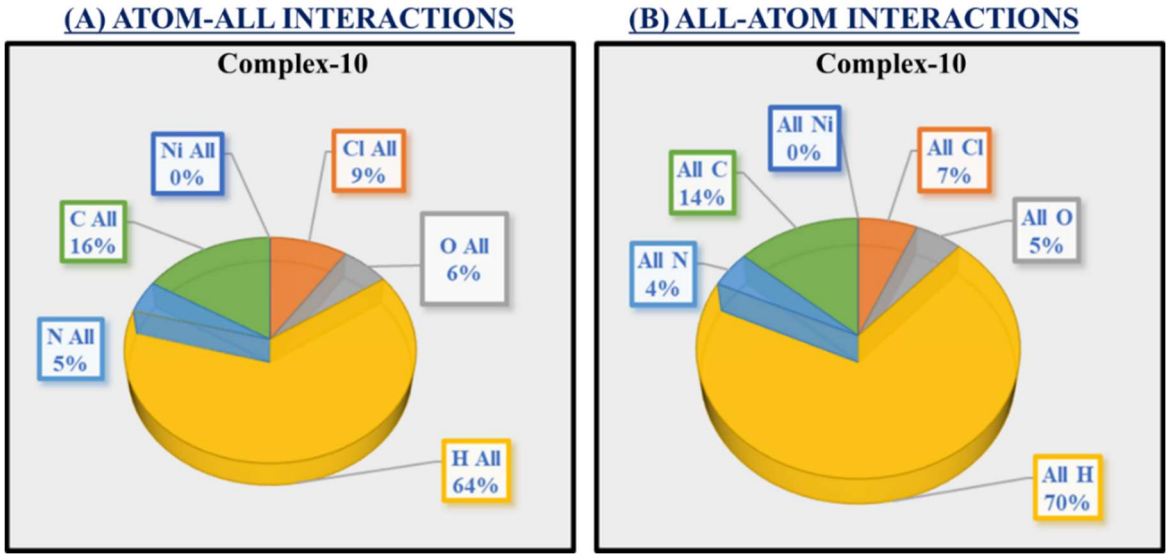

Fig.5.30. Graphical presentation of percentage interactions between each inside and outside atoms of complex-10

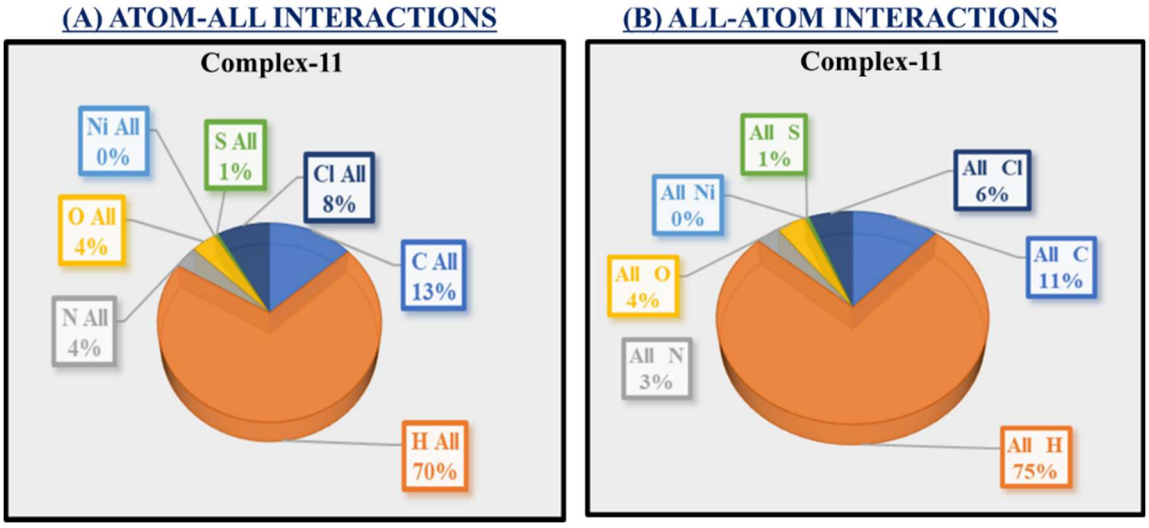

Fig.5.31. Graphical presentation of percentage interactions between each inside and outside atoms of complex-11

5.4 Conclusion

This research article demonstrates the derivatives of pyrazolone-based Ni(II) metal complexes. We investigated and successfully synthesized three octahedral Ni(II) complexes. Their characterization has been done using various analytical techniques. Spectral studies and X-ray single-crystal diffraction data demonstrate the ligand and solvent molecule coordinating through the oxygen atoms to Ni metal and reveal the octahedral geometry for three Ni(II) complexes. The powder XRD analysis was done for complex-**10** and complex-**11**. This proves that bulk products are the same as those in single-crystal form. This further shows that each complex has the same geometry and composition. Using a DFT method based on B3LYP/ LANL2DZ, the geometry was optimised, enabling the explanation of the frontier molecular orbitals of a molecule at a gaseous state. Significant findings by the HOMO-LUMO energy gap demonstrated the effectiveness of a complex-**10** because of the narrow energy gap, which allows the easy transport of electrons for charge transfer interactions within the molecule. Multiple interactions have been identified through Hirshfeld surface analysis. The magnetic study revealed the paramagnetic nature of complexes. The lower Racah parameter value for complex-**10** compared to the other two complexes suggests that complex-**10** has a more covalent and less ionic nature.

References

[1] M. Chakrabarty, A. Ahmed, R.A. Lal, Synthesis, Characterization, and Structural Assessment of Ni(II) Complexes Derived from Bis(2-hydroxy-1-naphthaldehyde)succinoyldihydrazone, Int. J. Inorg. Chem. 2015 (2015) 1–11. https://doi.org/10.1155/2015/121895.

[2] W. Derafa, D. Aggoun, Z. Messasma, S. Houchi, S. Bouacida, A. Ourari, An unexpected single crystal structure of nickel(II) complex: Spectral, DFT, NLO, magnetic and molecular docking studies, J. Mol. Struct. 1264 (2022) 133190. https://doi.org/10.1016/j.molstruc.2022.133190.

[3] M.F. Mahon, J. McGinley, K.C. Molloy, Synthesis and characterisation of metal complexes of pyrazole-derived ligands: Crystal structures of three nickel(II) complexes, Inorganica Chim. Acta. 355 (2003) 368–373. https://doi.org/10.1016/S0020-1693(03)00320-7.

[4] M.K. Szécsényi, V.M. Leovac, Z.K. Jacimovic, G. Pokol, TRANSITION METAL COMPLEXES WITH PYRAZOLE BASED LIGANDS with 3, 5-dimethyl-1-thiocarboxamidepyrazole, J. Therm. Anal. Calorim. 74 (2003) 943–952. https://akademiai.com/doi/pdf/10.1023/B%3AJTAN.0000011026.41481.bd.

[5] F. Marchetti, C. Pettinari, C. Di Nicola, A. Tombesi, R. Pettinari, Coordination chemistry of pyrazolone-based ligands and applications of their metal complexes, Coord. Chem. Rev. 401 (2019) 213069. https://doi.org/10.1016/j.ccr.2019.213069.

[6] E. González, A. Rodrigue-Witchel, C. Reber, Absorption spectroscopy of octahedral nickel(II) complexes: A case study of interactions between multiple electronic excited states, Coord. Chem. Rev. 251 (2007) 351–363. https://doi.org/10.1016/j.ccr.2006.08.011.

[7] I. Sheikhshoaie, N. Lotfi, J. Sieler, H. Krautscheid, M. Khaleghi, Synthesis, structures and antimicrobial activities of nickel(II) and zinc(II) diaminomaleonitrile-based complexes, Transit. Met. Chem. 43 (2018) 555–562. https://doi.org/10.1007/s11243-018-0241-5.

[8] S. Barad, K. Chaudhari, R.N. Jadeja, H. Roy, D. Choquesillo-Lazarte, Square pyramidal Cu(II) acylpyrazolone complex: Synthesis, characterization, crystal structure, DFT and Hirshfeld analysis, in-vitro anti-cancer evaluation, J. Mol. Struct.

1294 (2023) 136345. https://doi.org/10.1016/j.molstruc.2023.136345.

[9] S. Barad, K. Chaudhari, H. Roy, R.J. Butcher, R.N. Jadeja, Acylpyrazolone based Square pyramidal Cu(II) complexes: Synthesis, Structural characterization, DFT and antiproliferative properties, Inorganica Chim. Acta. 559 (2024) 121794. https://doi.org/10.1016/j.ica.2023.121794.

[10] S. Barad, K. Chaudhari, R.N. Jadeja, H. Roy, R.J. Butcher, Cytotoxicity assay and gene expression studies of acylpyrazolone-based square planar Cu(II) complexes: synthesis, characterization and computations, J. Coord. Chem. 76 (2023) 1955–1983. https://doi.org/10.1080/00958972.2023.2289004.

[11] M. Travadi, R.N. Jadeja, R.J. Butcher, M.S. Shekhawat, Neodymium based acylpyrazolone complexes: Synthesis and physicochemical characterizations, Inorganica Chim. Acta. 559 (2024) 121766. https://doi.org/https://doi.org/10.1016/j.ica.2023.121766.

[12] I. Shaikh, R.N. Jadeja, R. Patel, Three mixed ligand mononuclear Zn(II) complexes of 4-acyl pyrazolones: Synthesis, characterization, crystal study and anti-malarial activity, Polyhedron. 183 (2020) 114528 https://doi.org/10.1016/j.poly.2020.114528.

[13] I.U. Shaikh, Synthesis , Characterization and Studies on d^{10} Metal Complexes derived from Acyl Pyrazolones, (2020).

[14] G.M. Sheldrick, Crystal structure refinement with SHELXL, Acta Crystallogr. Sect. C Struct. Chem. 71 (2015) 3–8. https://doi.org/10.1107/S2053229614024218.

[15] G.M. Sheldrick, SHELXT - Integrated space-group and crystal-structure determination, Acta Crystallogr. Sect. A Found. Crystallogr. 71 (2015) 3–8. https://doi.org/10.1107/S2053273314026370.

[16] Y. El Bakri, S.K. Mohamed, A. Ahsin, S. Karthikeyan, S. Abuelhassan, A.E. Abdel-Rahman, I.S. Marae, E.A. Bakhite, J.T. Mague, R. Al-Salahi, Synthesis, crystal structure investigation, Hirshfeld and DFT studies of newly synthesized dihydroisoquinoline derivatives, Arab. J. Chem. 16 (2023) 105294. /https://doi.org/10.1016/j.arabjc.2023.105294.

[17] C.F. Macrae, P.R. Edgington, P. McCabe, E. Pidcock, G.P. Shields, R. Taylor, M. Towler, J. Van De Streek, Mercury: Visualization and analysis of crystal structures,

J. Appl. Crystallogr. 39 (2006) 453–457. https://doi.org/10.1107/S002188980600731X.

[18] J.M.M. and R.C.M. PRADEEP KUMAR VISHWAKARMA, Pyrone-based Cu (II) complexes , their characterization , DFT based conformational drift from square planar to square pyramidal geometry, 128 (2016) 511–522. https://doi.org/10.1007/s12039-016-1048-6.

[19] S. Parihar, S. Pathan, R.N. Jadeja, A. Patel, V.K. Gupta, Synthesis and Crystal Structure of an Oxovanadium(IV) Complex with a Pyrazolone Ligand and Its Use as a Heterogeneous Catalyst for the Oxidation of Styrene under Mild Conditions, Inorg. Chem. 51 (2012) 1152–1161. https://doi.org/10.1021/ic202396q.

[20] W.J. Geary, The use of conductivity measurements in organic solvents for the characterisation of coordination compounds, Coord. Chem. Rev. 7 (1971) 81–122. https://doi.org/10.1016/S0010-8545(00)80009-0.

[21] R.N. Patel, Y. Singh, Y.P. Singh, R.J. Butcher, Synthesis, crystal structure and DFT calculations of octahedral nickel(II) complexes derived from N′-[(E)-phenyl(pyridin-2-yl)methylidene]benzohydrazide, J. Coord. Chem. 69 (2016) 2377–2390. https://doi.org/10.1080/00958972.2016.1189543.

[22] A.P. Mishra, R. Mishra, R. Jain, S. Gupta, Synthesis of new VO(II), Co(II), Ni(II) and Cu(II) complexes with Isatin-3-chloro-4-floroaniline and 2-pyridinecarboxylidene-4-aminoantipyrine and their antimicrobial studies, Mycobiology. 40 (2012) 20–26. https://doi.org/10.5941/MYCO.2012.40.1.020.

[23] D. Schweinfurth, J. Krzystek, I. Schapiro, S. Demeshko, J. Klein, J. Telser, A. Ozarowski, C.Y. Su, F. Meyer, M. Atanasov, F. Neese, B. Sarkar, Electronic structures of octahedral Ni(II) complexes with “click” derived triazole ligands: A combined structural, magnetometric, spectroscopic, and theoretical study, Inorg. Chem. 52 (2013) 6880–6892. https://doi.org/10.1021/ic3026123.

[24] M. Dalal, Calculation of Dq, B and β Parameters, I (n.d.).

[25] R. Stranger, K.L. McMahon, L.R. Gahan, J.I. Bruce, T.W. Hambley, Spin-Orbit Mixing and Nephelauxetic Effects in the Electronic Spectra of Nickel(II)-Encapsulating Complexes Involving Nitrogen and Sulfur Donors, Inorg. Chem. 36 (1997) 3466–3475. https://doi.org/10.1021/ic9614531.

[26] O. Domanov, E. Weschke, T. Saito, H. Peterlik, T. Pichler, M. Eisterer, H. Shiozawa, Exchange coupling in a frustrated trimetric molecular magnet reversed by a 1D nanoconfinement, Nanoscale. 11(22) (2019). http://dx.doi.org/10.1039/C9NR00796B.

[27] S. Mugiraneza, A.M. Hallas, Magnetic Susceptibility Data With the Curie-Weiss law (2022)5:95. https://doi.org/10.1038/s42005-022-00853-y.

[28] Y.P. Singh, R.N. Patel, Y. Singh, Crystal structure, configurational and DFT study of nickel(II) complexes with N2O-donor type Schiff base ligand, Indian J. Chem. - Sect. A Inorganic, Phys. Theor. Anal. Chem. 57A (2018) 44–51.

[29] P.J. Hay, W.R. Wadt, Ab initio effective core potentials for molecular calculations. Potentials for the transition metal atoms Sc to Hg, J. Chem. Phys. 82 (1985) 270–283. https://doi.org/10.1063/1.448799.

[30] M. Travadi, R.N. Jadeja, R.J. Butcher, Synthesis, Covalency Sequence, and Crystal Features of Pentagonal Uranyl Acylpyrazolone Complexes along with DFT Calculation and Hirshfeld Analysis, ACS Omega. 7 (2022) 34359–34369. https://doi.org/10.1021/acsomega.2c03923.

[31] M.S. Jana, A.K. Pramanik, T.K. Mondal, Octahedral Ni(II) and Cu(II) complexes with a new hexadentate (NSN) 2 donor ligand: Synthesis, characterization, X-ray structure and DFT calculations, Polyhedron. 76 (2014) 29–35. https://doi.org/10.1016/j.poly.2014.03.052.

[32] J. Ghannam, T. Al Assil, T.C. Pankratz, R.L. Lord, M. Zeller, W.T. Lee, A Series of 4- and 5-Coordinate Ni(II) Complexes: Synthesis, Characterization, Spectroscopic, and DFT Studies, Inorg. Chem. 57 (2018) 8307–8316. https://doi.org/10.1021/acs.inorgchem.8b00958.

[33] S.A. Alramadhan, H.H. Hammud, B.F. Ali, H.A. Ghabbour, S. Sarfaraz, K. Ayub, Structures, Characterization and DFT Studies of Four Novel Nickel Phenanthroline Complexes, Crystals. 13 (2023). https://doi.org/10.3390/cryst13050738.

[34] S. Belošević, M.M. Vasojević, M.S. Jeremić, A. Meetsma, Z.D. Matović, Preparation, configurational and DFT-NBO analysis of nickel(II) complexes with edta-type ligands containing six-membered backbone ring: Crystal structure of [Ni(H 2O) 6][Ni(1,3-pdta)]·2H 2O, J. Coord. Chem. 66 (2013) 1730–1745.

https://doi.org/10.1080/00958972.2013.789104.

[35] M.A. Spackman, D. Jayatilaka, Hirshfeld surface analysis, CrystEngComm. 11 (2009) 19–32. https://doi.org/10.1039/b818330a.

[36] N.H. Nasaruddin, S.N. Ahmad, S.S. Sirat, K.W. Tan, N.A. Zakaria, S.S. Mohamad Nazam, N.M.M.A. Rahman, N.S. Mohd Yusof, H. Bahron, Synthesis, Structural Characterization, Hirshfeld Surface Analysis, and Antibacterial Study of Pd(II) and Ni(II) Schiff Base Complexes Derived from Aliphatic Diamine, ACS Omega. 7 (2022) 42809–42818. https://doi.org/10.1021/acsomega.2c04688.

[37] P.R. Spackman, M.J. Turner, J.J. McKinnon, S.K. Wolff, D.J. Grimwood, D. Jayatilaka, M.A. Spackman, CrystalExplorer: A program for Hirshfeld surface analysis, visualization and quantitative analysis of molecular crystals, J. Appl. Crystallogr. 54 (2021) 1006–1011. https://doi.org/10.1107/S1600576721002910.

[38] U.M. Osman, S. Silvarajoo, M.F. Noor Hassim, S. Arshad, A.H. Anizaim, F.I. Abdul Razak, Synthesis, X-Ray Structure, Hirshfeld Surface Analysis, DFT Calculations, and Molecular Docking Studies of Nickel(II) Complex with Thiosemicarbazone Derivative, Bioinorg. Chem. Appl. 2021 (2021). https://doi.org/10.1155/2021/5536902.

[39] P. Lakshmanan, E. Gayathri, S. Thirumaran, S. Ciattini, Synthesis, crystal structure, DFT and Hirshfeld surface analysis of Ni(II) complexes: Precursor for nickel sulfide nanoparticles, J. Mol. Struct. 1273 (2023) 134306. https://doi.org/10.1016/j.molstruc.2022.134306.

Published Paper

Journal of Molecular Structure 1321 (2025) 140213

Contents lists available at ScienceDirect

Journal of Molecular Structure

journal homepage: www.elsevier.com/locate/molstr

Chemical assessment of three octahedral Ni(II) complexes with heterocyclic acylpyrazolone ligand: Crystal structure, DFT-NBO analysis, Hirshfeld and Magnetic study

Sapna Barad [a], Siddharth Saurabh [a], Duane Choquesillo-Lazarte [b], Rajendrasinh N. Jadeja [a,*]

[a] Department of Chemistry, Faculty of Science, The Maharaja Sayajirao University of Baroda, Vadodara 390002, India
[b] Laboratorio de Estudios Cristalograficos, IACT, CSIC-Universidad de Granada, Av. De las palmeras 4, E-18100, Armilla, Granada, Spain

ARTICLE INFO

Keywords:
Computational study
Magnetic study
Single crystal
Octahedral Ni(II) complex

ABSTRACT

We have synthesized three novel mononuclear Nickel(II) coordination complexes [Ni(DMBPTMP)$_2$(EtOH)$_2$], [Ni(PCBPMP)$_2$(DMF)(H$_2$O)] and [Ni(PCBPTMP)$_2$(DMSO)$_2$] with σ-donating acylpyarazolone ligands. All the complexes have been comprehensively characterized via FTIR, UV–Vis, TGA, and Magnetic study. Additionally, single crystal X-ray diffraction analysis was successfully used to characterize the three complexes. The findings showed that the geometry around Ni(II) is slightly distorted octahedral in [Ni(DMBPTMP)$_2$(EtOH)$_2$], [Ni(PCBPMP)$_2$(DMF)(H$_2$O)] complexes and also in the centrosymmetric [Ni(PCBPTMP)$_2$(DMSO)$_2$] complex. In all the complexes the metal is bischelated by two pyrazolone molecules via carbonyl and benzoyl carbonyl oxygen donors, but with a different configuration of ligands. In addition to the experimental studies and spectroscopic characteristics, DFT computational analysis and Natural bonding orbital (NBO) analysis have been performed using a B3LYP/LANL2DZ basis set for the optimization. All three Ni(II) complexes give three distinct absorption transitions which has been proved by Electronic spectral analysis. A paramagnetic nature of the complex is confirmed through magnetic study. Utilising Hirshfeld surface analysis, intermolecular interactions of complexes were evaluated.

1. Introduction

The catalytic and bioinorganic significance of transition metal complexes has sparked considerable interest in their chemistry. Coordination compounds, which form coordinate bonds with donor atoms like sulfur, oxygen, and nitrogen, have a rich history [1]. Coordination chemistry involves metal ions accepting electron pairs from adjacent ligands. Due to their potential applications in magnetic ordering, catalysis, and biological mimicking, significant research has been dedicated to synthesizing and characterizing polynuclear transition metal complexes and examining their magnetic and electronic properties over the past few decades [2]. Nickel is a key transition metal, with Nickel(II) being more stable than its other oxidation states: Nickel(0), Nickel(I), Nickel(III), and Nickel(IV). Nickel(II) complexes can adopt various geometries, including square planar, tetrahedral, trigonal bipyramidal, and octahedral, with octahedral and square planar being the most common. The distinct chemical and physical properties of each Nickel(II) complex, determined by its specific ligand, make their study both fascinating and challenging [3].

In many fields of material chemistry, Nickel is an essential metal. The production of ceramics using nickel-containing alkoxides involves contemporary interactions between nickel coordination chemistry and material science. This process utilizes the distinctive properties of nickel alkoxides to create advanced ceramic materials [4]. However, It is well known that pure inorganic nickel salts or the dehydroacetic acid ligand alone are less active than nickel complexes containing Ni^{2+} [5]. Being more stable than Nickel(0), Nickel(I), Nickel(III) and Nickel(IV), Nickel is commonly found in nature as Nickel(II). The distinct chemical and physical properties of every Nickel(II) complex paired with a specific ligand make their investigation interesting and daunting [3].

In recent years, the coordination chemistry of pyrazoles and other nitrogen-containing heterocyclic compounds has garnered significant

Abbreviations: DMBPTMP, 4-(3,5-dimethyl benzoyl 1-(p-tolyl) 3-methyl 5-pyrazolone; PCBPTMP, p-chlorobenzoyl 1-(p-tolyl) 3-methyl 5-pyrazolone; PCBPMP, p-chlorobenzoyl 1- phenyl 3-methyl 5-pyrazolone.

* Corresponding author at: Department of Chemistry, Faculty of Science, The Maharaja Sayajirao University of Baroda, Vadodara 390002, India.
E-mail addresses: sapna.b-chem@msubaroda.ac.in (S. Barad), duane.choquesillo@csic.es (D. Choquesillo-Lazarte), rjadeja-chem@msubaroda.ac.in (R.N. Jadeja).

https://doi.org/10.1016/j.molstruc.2024.140213
Received 16 May 2024; Received in revised form 23 September 2024; Accepted 26 September 2024
Available online 5 October 2024